A hypomorphic *Stip1* allele reveals the requirement for chaperone networks in mouse development and aging

Rachel E. Lackie[1,2], Marilene H. Lopes[1,3], Sali M.K. Farhan[4], Abdul Razzaq[1,2], Gilli Moshitzky[5], Mariana Brandao Prado[3], Flavio H. Beraldo[1,7], Andrzej Maciejewski[1,6], Robert Gros[1,7,8], Jue Fan[1], Wing-Yiu Choy[6], David S. Greenberg[5], Vilma R. Martins[11], Martin L. Duennwald[9,10], Hermona Soreq[5], Vania F. Prado[1,2,7,10*], Marco. A.M. Prado[1,2,7,10 *]

[1]Molecular Medicine, Robarts Research Institute, [2]Program in Neuroscience, University of Western Ontario, [3]Laboratory of Neurobiology and Stem cells, Department of Cell and Developmental Biology; Institute of Biomedical Sciences, University of Sao Paulo,[4]Analytic and Translational Genetics Unit, Center for Genomic Medicine, Massachusetts General Hospital, Harvard Medical School, and The Stanley Center for Psychiatric Research, Broad Institute of MIT and Harvard, Boston, MA, USA, [5]The Edmond and Lily Safra Center for Brain Sciences, Department of Biological Chemistry, The Alexander Silberman Institute of Life Sciences, The Hebrew University of Jerusalem, [6]Department of Biochemistry, [7] Department of Physiology and Pharmacology, [8]Department of Medicine, [9]Department of Pathology and Laboratory Medicine, [10] Department of Anatomy & Cell Biology, Schulich School of Medicine and Dentistry, University of Western Ontario, London Ontario, Canada. [11]International Research Center, A.C.Camargo Cancer Center, São Paulo, Brazil.

- **Correspondence:**
  Dr. Marco A.M. Prado
  mprado@robarts.ca
- Dr. Vania F Prado
- vprado@robarts.ca

Robarts Research Institute
1151 Richmond St. N, N6A 5B7
The University of Western Ontario
London, Ontario, Canada
Tel: 519-9315777 Ext. 24888 or 24889

Short title: STI1 in mammalian proteostasis

Keywords: Aging / Hsp70 / Hsp90 / Proteostasis / STI1/ stem cells/STIP1/HOP/ Neurodegeneration

ABSTRACT

The chaperone machinery is well conserved from yeast to mammals, however our knowledge of their impact on mammalian physiology is lagging. Stress-inducible phosphoprotein-1 (STI1; STIP1; Hop) is a co-chaperone that simultaneously interacts with Hsp70 and Hsp90 via three tetratricopeptide repeat (TPR) domains, of which TPR1 and TPR2B may be redundant in yeast. In-depth analysis of human datasets indicated that STI1 belongs to a set of co-chaperones that is essential in humans and that the TPR1 domain is evolutionarily conserved, suggesting that in mammals it may be required for optimal STI1 activity *in vivo*. We generated mice with a hypomorphic *Stip1* allele lacking the TPR1 domain. While these mice are viable, they presented decreased levels of Hsp90 client proteins and co-chaperones, suggesting profound dysregulation of chaperone networks. We used this hypomorphic STI1 mutant mouse line to investigate the requirement of STI1-mediated regulation of chaperone networks in mouse physiology. Embryonic cell pluripotency was severely affected by decreased STI1 activity, contributing to the abnormal development in these mice. Moreover, adult TPR1-deprived STI1 mice presented age-related hippocampal neurodegeneration, resulting in compromised memory recall. Our findings reveal a requirement for optimal regulation of chaperone networks and their clients during development and strict dependence on full STI1 activity for healthy neuronal aging. These experiments demonstrate the unique experimental power of using hypomorphic alleles to reveal how chaperone networks regulate mammalian physiology.

INTRODUCTION

Regulation of proteostasis by the Heat-shock protein 70 (Hsp70) and 90 (Hsp90) is thought to be particularly important during development [1,2], aging [3] and in neurodegenerative diseases [4-6]. The heat shock response, mainly controlled by the transcription factor *Hsf1*, protects organisms from different types of insults and thus modulates resilience in adulthood [7]. Also, Hsp90 and Hsp70 help to buffer deleterious changes due to genetic mutations and both chaperones seem to contribute to phenotypic variability [8,9]. However, despite our extensive knowledge of the roles of chaperone networks in yeast and worms, how chaperones and co-chaperones regulate physiological processes *in vivo* in mammals is not fully appreciated.

Stress-inducible phosphoprotein 1 (STI1, STIP1 or Hop for Hsp organizing protein in humans) is a co-chaperone that regulates the transfer of client proteins between Hsp70 and Hsp90 [10-13]. STI1 is a modular protein containing three tetratricopeptide repeat domains (TPR1, TPR2A and TPR2B), which interact with Hsp70 (TPR1 and TPR2B) and Hsp90 (TPR2A), respectively [11]. STI1 and its TPR domains are conserved from yeast to humans. The TPR2A and TPR2B domains are required for activation of client proteins [11,13,14]. In contrast, the TPR1 domain is absent in *C. elegans* [15], and it may be dispensable in yeast, as mutant STI1 protein lacking the TPR1 domain is functional, albeit with decreased efficiency in forming ternary complex with Hsp70 and Hsp90 [13]. Hence, STI1 has a unique role in the chaperone cycle, but the function of its TPR1 domain remains poorly understood.

Although deletion of STI1 in yeast is not lethal, it causes growth impairments in challenging conditions [16]. Also, yeast STI1 interacts genetically with Hsp90, and deletion of STI1 sensitizes yeast to Hsp90 suppression [17-20], illustrating the complex relationship between

these proteins. Elimination of STI1 in *C. elegans* is not lethal, but it causes deficits in reproduction, longevity and resilience to thermal stressors [15]. In mice, deletion of STI1 affects the rate of blastocyst survival and escaping embryos died early in development (E10.5), indicating that STI1 is essential in mammals [2].

We surveyed human and mouse databases and found important differences between mammalian and yeast dependence on co-chaperones for survival. To further unveil the impact of chaperones in mammalian physiology, we engineered a mouse line with a STI1 hypomorphic allele coding for a protein lacking the TPR1 domain. Our results reveal that optimal STI1 activity *in vivo* is required to maintain the functionality of chaperone networks with impact in pluripotency during development and in neuronal aging. This new STI1 hypomorphic mouse line opens new avenues to understand the role of chaperone networks in maintaining client protein levels in different tissues in response to physiological and pathological challenges.

RESULTS

STIP1 loss-of-function mutations in humans are rare

Loss of STI1 is tolerated in yeast [16] and *C. elegans* [15,21], but knockout of *Stip1* in mice causes embryonic lethality [2]. To determine whether STIP1 in humans may also be essential, we determined the frequency of variation in *STIP1* in relatively healthy individuals using public databases, aggregating genetic information from thousands of exomes and genomes such as ExAC (60,706 individuals) and gnomAD (138,632 individuals) [22]. Protein truncation variants (PTVs) are a class of mutations that typically lead to loss of protein function and can reveal the biological consequences of gene deficiency in humans. After filtering for false PTVs, we have observed 1 and 4 heterozygous *STIP1* PTV carriers in ExAC and gnomAD, respectively, at a frequency of <<0.001% (Supplementary Table 1). In comparison, *HSP90AA1* presented 8 and 22 PTVs in ExAC and gnomAD, respectively, at a 10-fold higher frequency of <0.01% (Supplementary Table 1). While we applied strict false positive PTV filtering criteria (see methods), we are unable to confirm whether these PTVs are real or are the result of sequencing or alignment errors. However, the *STIP1* pLI score, which reflects the probability that a given gene is intolerant to loss-of-function variation (haploinsufficient) was 1. This suggested that loss-of-function variations in *STIP1* are most likely not tolerated in humans or may result in a disease phenotype [22]. In comparison, the pLI score of *HSP90AA1*, the stress inducible Hsp90 allele, was 0.68, suggesting that PTVs may be tolerated in *HSP90AA1*. This is likely due to compensation by the highly redundant *HSP90AB1*, the constitutive Hsp90 isoform. Interestingly, the *HSP90AB1* pLI score is 1. These analyses mirrored the survival of STI1, Hsp90α and Hsp90β knockout mice [2,23,24]. Whereas Hsp90α knockout mice survive to adulthood [23], both STI1 and Hsp90β gene ablation causes embryonic lethality [2,24]. We also surveyed the following

disease-based databases: GWAS Catalog, ClinVar, HGMD, and DECIPHER, to determine if variation in *STIP1* or *HSP90AA1*, *HSP90AB1* have been reported. We did not observe any PTVs in these genes; however, we observed cases with copy number variation (gain and loss) of large genomic regions spanning >30-1500 genes.

We extended our analysis to other Hsp90 co-chaperones to determine whether they may be redundant in mammals by comparing human genetic data with viability of published knockout mice. We surmised that genes with high pLI that show lethality when knocked out in mice or other organisms are likely non-redundant in humans. p23 (*PTGES3*) is a co-chaperone that enters the Hsp90 cycle late to reduce Hsp90 ATPase activity [25,26]. Its pLI is 0.87, which is borderline for loss-of-function tolerability (pLi>0.9), however mice null for *PTGES3* die after birth due to defective lung development [26], indicating that p23 activity is not redundant and loss-of-function mutations may not be tolerated in humans. Aha1 (*AHSA1)*, activates Hsp90 ATPase activity regulating the chaperone cycle and it can also displace STI1 [27,28]. *AHSA1* has a pLI score of 0.94, suggesting the possibility that it is a required gene in mammals as well. Unfortunately, although knockout mice have been generated for Aha1 as part of the KOMP initiative, phenotypes have not yet been described. In contrast, *FKBP5* has a pLI of 0.50, which aggress with the viability of knockout mice [29]. *CDC37*, a co-chaperone that is required for the recruitment and maturation of kinases but also has more complex activities [30] has pLI of 0.96, indicating intolerance for loss-of-function in mammals, and indeed loss of *CDC37* is lethal in *C. elegans* and yeast [31]. Searches in the MGI database did not reveal available CDC37 knockout mice. *SGTA* showed a pLI of 0.47, suggesting that mammals may tolerate loss-of-function mutations for this co-chaperone, and in fact, *SGTA* knockout mice are viable [32]. We identified a discrepancy between our database analysis and mammalian viability as determined by using

knockout mice for *PPP5c*, which has a pLI = 1. In contrast to the potential intolerance for human PTVs, knockout mice for *PPP5c* are viable [33]. Figure 1 A-C illustrates functional and physical interactions amongst these genes. Supplementary Table 1 tabulates the observed PTVs, SNVs, indels, CNVs, and associations, providing a comprehensive summary of the genes above using publicly available datasets of healthy controls and disease-ascertained individuals. Collectively, our analysis indicates that constitutive Hsp90, STI1, CDC37, AHA1 and p23 are essential in mammals.

ΔTPR1 mice

To investigate the relationship between STI1 and the chaperone network in mammals and, in particular, the role of the TPR1 domain for STI1 activity *in vivo*, we generated TPR1-deprived STI1 mice using the Cre/lox system (Fig 2A and B). Homozygous mutant STI1 mice (ΔTPR1 mice) were viable, although they were smaller than their control littermates (Fig 2C). At embryonic day E17.5, the proportion of homozygous ΔTPR1 mutants was close to the expected Mendelian frequency of 25% (Supplementary Table 2). However, the frequency of homozygous newborn ΔTPR1 mice was lower than expected [Supplementary Table 2, 15% instead of 25%, $\chi2$ (1, N=246) = 14.89, $p<0.001$], and their survival was lower than the expected Mendelian frequency [$\chi2$ (3, N=54) = 37.111, $p<0.001$]. This suggested that a small proportion of homozygous mutants were dying after birth, likely due to sibling competition. Nonetheless, homozygous ΔTPR1 mice that survived the first few days thrived and reached adulthood (Fig 2C and D). The ΔTPR1 protein was at least partially functional *in vivo*, as having one *ΔTPR1* allele rescued the early embryonic lethality of STI1 null mutants (Supplementary Table 3).

ΔTPR1 mice weighed less than littermate controls starting at birth and continued to gain less weight during adulthood (Fig 2D). To further examine this potential metabolic phenotype, we

tested mice using metabolic cages. ΔTPR1 mice were hyperactive even when they habituated to their environment (Fig 2E, p=0.043 for light phase and p=0.069 for dark phase) and showed higher oxygen consumption (Fig 2F, p<0.001 for both light and dark phase) and CO_2 production (Fig 2G, p=0.002 for light cycle, p<0.0001 for dark cycle) than control littermates. Respiratory exchange ratio was not significantly different between genotypes due to increase in both O_2 consumption and CO_2 production (Supplementary Fig 1A, p=0.17 for light phase, p=0.11 for dark phase). On measures of energy expenditure (body heat), there was no difference between genotypes in either the light cycle (Supplementary Fig 1B p= 0.10) or the dark cycle (Supplementary Fig 1C p=0.60). Food consumption (Supplementary Fig.1C light cycle: p= 0.41, dark cycle p= 0.26) and water consumption (Supplementary Fig 1D light cycle: p=0.54, dark cycle: p=0.30) were identical between genotypes, suggesting that the decreased weight of ΔTPR1 mice may be linked to their increased activity and energy expenditure. In the dark cycle, ΔTPR1 mice slept significantly less, measured as immobility bouts, than control littermates (p=0.013). However, during the period that mice usually sleep (light cycle) there were no differences between genotypes (p=0.28, Supplementary Fig 1E). This result agrees with the increased ambulatory activity of STI1 mice.

We used qPCR to determine mRNA expression for the mutated locus (Fig 2H-I). Analysis with primers targeting exons 2&3 (detects full length STI1 mRNA, but not ΔTPR1 STI1 mRNA) showed 50% reduction in full length STI1 mRNA levels in heterozygous mutants, whereas in homozygotes mutants, full length STI1 mRNA was not detected in adult cortical tissue (Fig 2H, p<0.0001, similar results were obtained for MEFs, Supplementary Fig 2). Importantly, primers flanking exons 8&9 (which detect both full length and ΔTPR1 STI1 mRNA) showed that heterozygous and homozygous mutant mice expressed similar levels of STI1 mRNA as WT

mice, indicating that expression of the ΔTPR1 STI1 mRNA was similar to that of full length STI1 mRNA (Fig 2I, $p>0.05$).

Immunoblot analysis demonstrated that STI1 protein levels in ΔTPR1 homozygous mice had a reduced molecular mass of 53 kDa (Fig 2L). The deleted TPR1 domain is predicted to be 12-13 kDa in size, hence the mutant protein matches the expected molecular mass (66 kDa minus 13 kDa). We detected close to 80% reduction of the mutant protein levels when compared to WT littermates (Fig 2M, $p<0.0001$), supporting the notion that ΔTPR1 translation, due to the absence of a KOZAK sequence, was affected. In heterozygous ΔTPR1 mice the levels of wild-type and mutated proteins were half as much as that of wild-type or ΔTPR1 homozygous mice, respectively. Control experiments demonstrated that our polyclonal antibody recognizes several epitopes on the STI1 protein, therefore excluding the possibility that the reduced levels of immunostaining observed were due to decreased binding of the antibody to deleted epitopes (Supplementary Fig 2C).

Abnormal chaperone network in ΔTPR1 mice

To determine the impact of the ΔTPR1 protein on the chaperone system, we examined the expression levels of the two major chaperone partners of STI1, Hsp70 and Hsp90. We focused more specifically on Hsp90β because previous experiments in mice overexpressing STI1 detected increased levels of this constitutive Hsp90 protein [34]. We did not find any changes when we compared levels of Hsp70 and Hsp90 mRNA ($p=0.37$ and $p=0.18$) and protein ($p=0.07$ for pan Hsp90, $p=0.46$ for Hsp90β) in homozygous ΔTPR1 and littermate control mice ($p=0.068$, Fig 2J, K, N-Q). Immunostaining for STI1, Hsp70 and Hsp90 in MEFs revealed that there were no alterations of localization for the two chaperones and that mutated STI1 levels in MEFs were reduced as expected (Supplementary Fig 2D and E).

To start to unveil whether STI1 regulates chaperone network function, we investigated mRNA and protein levels for co-chaperones and client proteins. Because inhibition of Hsp90 activity could alter gene expression [35], we performed non-biased RNA-sequencing analysis, to test the possibility that in mutant mice there are general transcriptome changes that can contribute to phenotypes. Long RNA-sequencing was performed on 5 cortex samples from STI1 control and 5 STI1 homozygous ΔTPR1 mice. RIN values for these samples ranged between 8.2 and 8.7. Illumina sequencing yielded an average of 797,963 reads per sample, with 93.69% reads mapping rate to the mouse genome. We confirmed the complete absence of STI1 exons 2 and 3 on ΔTPR1 samples compared to wild-type control tissues (Supplementary Fig 3). Principal component analysis and sample distance matrix analyses did not segregate between the two groups, indicating minimal differences between the two genotypes at the transcriptome level (Supplementary Fig 3). Furthermore, RNA sequencing analysis did not reveal any significant changes in transcripts passing FDR correction (padj<0.05). Hence, it is unlikely that general transcriptome changes contributed to phenotypes in ΔTPR1 mice.

The activity of HSF1, a transcription factor that regulates heat shock genes such as Hsp70 and Hsp90 [36], is increased upon inhibition of Hsp90 activity and regulates the heat shock response [37-41]. We measured HSF1 protein levels in brain cortical extracts to determine if heat shock response was affected in mutant mice. We detected no difference in HSF1 protein levels (Fig 3A and B) between control and ΔTPR1 homozygous or heterozygous mouse tissue (p=0.6 for WT vs homozygous ΔTPR1 mutants, One-way ANOVA). This result agreed with the observation of relatively normal levels of Hsp90 and Hsp70, suggesting that the heat shock response was not abnormally activated in ΔTPR1 mice. We also examined the levels of Hsp40 (Fig 3A and C), a DnaJ protein that is involved in regulating Hsp70 function and it is present in the complex of

Hsp70-STI1 [42-45]. Likewise, there was no significant change in Hsp40 protein levels ($p>0.1$). Moreover, the peptidyl-prolyl isomerase (PPIase) Hsp90 co-chaperone FKBP51, involved in maturation of steroid hormone receptors and stabilization of Tau species [46-49], presented normal levels (Fig 3D and E, $p=0.4$).

We followed this initial analysis by investigating the levels of Hsp90 clients. Inhibition of STI1 activity or reduced STI1 levels decreased the levels of Hsp90 client proteins in mammalian cells [2,50,51]. We first tested the transcripts for glucocorticoid receptor, Tau protein and G protein-coupled receptor kinase 2 (GRK2), all classical Hsp90 client proteins, by qPCR analysis. This experiment indicated that the mRNA levels for these three classical Hsp90 clients are not altered in brain tissue of ΔTPR1 mice (Supplementary Fig 4A-C, $p=0.47$ for GR, $p=0.33$ for Tau, $p=0.20$ for GRK2). In contrast, Western blot analyses showed that these Hsp90 client proteins were very sensitive to reduced levels of mutated STI1. For example, GR was conspicuously decreased even in heterozygous ΔTPR1 tissue, (Fig 4A and B, $p<0.0001$, for heterozygous and homozygous mice). Tau was also reduced, (Fig 4A and C) in heterozygous ($p=0.0039$) and homozygous mutants ($p=0.0223$). In contrast, GRK2 was only reduced in tissues from homozygous ΔTPR1 mice (Fig 4A and D, $p=0.039$).

To further understand how ΔTPR1 protein affects chaperone networks, we investigated a number of proteins involved in Hsp90 function. Pin1, which interacts with Hsp90 in the final stages of protein folding and maturation [46], presents 50% reduction in both heterozygous and homozygous mutants compared to littermate controls (Fig 4E and G, $p<0.0001$, $p<0.0001$ respectively). Cyclophilin A (CypA), another PPIase, presented 75% reduction in protein levels in heterozygous and homozygous mutants (Fig 4E and H, $p=0.0007$, $p=0.0008$).

In addition to finding that several proteins with PPIase activity present significant dependence on STI1, we also found that the co-chaperone C-terminal Hsp70 Binding protein (CHIP), an ubiquitin E3 ligase that sorts chaperone-mediated protein degradation, presents 40% reduction in heterozygous and homozygous ΔTPR1 mice compared to littermate controls (Fig 4E and F, p=0.0077, p=0.0018). CHIP also contains TPR domains and can compete with STI1 for binding to Hsp90, promoting proteasomal degradation of several client proteins [52,53]. In agreement with the possibility of disturbed proteostasis and our RNA-Seq data, we found no significant changes in mRNA expression for any of these genes (Supplementary Fig 4D-H).

We next sought to determine whether the altered steady state levels of clients and Hsp90-interacting proteins is a result of reduced STI1 levels or TPR1-deficient STI1 contributes to this decrease in heterozygous tissue. To this end we compared the expression of clients and co-chaperones affected by the ΔTPR1 protein in tissues from mice with 50% reduction of STI1 wild-type levels [STI1 heterozygous KO mice [2,34]], without the expression of ΔTPR1 protein. Interestingly, in heterozygous STI1 knockout mice, we observed no significant changes in Hsp90 client protein expression, indicating that loss of 50% of STI1 levels does not seem to affect client protein stability (Fig 5A-C). Likewise, we investigated Hsp90 accessory protein levels in STI1 heterozygous mice. In contrast to our findings in ΔTPR1 mouse tissue, increased levels of accessory proteins were found in STI1 heterozygous KO mice: FKBP51 (p=0.0008), Pin1 (p=0.014), CHIP (p=0.0215) and CypA (p=0.002, Fig 5D-H), suggesting that 50% reduction in STI1 can be compensated in heterozygous STI1-null mice. Therefore, changes in protein levels in heterozygous ΔTPR1 mice differ substantially from heterozygous STI1 knockout mice.

We considered the possibility that in heterozygous ΔTPR1 mice the presence of the mutated protein somehow decreased the activity of the chaperone machinery, even in the presence of the

wild-type protein. If that is correct, ΔTPR1 mice should reflect changes that are more similar to the loss of STI1, suggesting that ΔTPR1 may represent a functional hypomorph. As STI1-KO embryos and STI1-KO MEFs are not viable (Beraldo et al, 2013), we generated a cell line lacking STI1 to test whether the changes we observed in ΔTPR1 mice approximate loss of STI1 function [2]. We generated a STI1-KO neuronal cell line (SN56KO cells) using CRISPR-Cas9 technology (Supplementary Fig 5), anticipating that a cell line may be more resistant to the loss of STI1 than MEFs. Interestingly, although SN56KO cells showed increased cell death both under normal culture conditions and under treatment with the apoptosis inducer staurosporine when compared to control cells (data not shown), they could survive in culture in contrast to KO MEFs. As expected, the levels of Hsp90 and Hsp70 were not different between knockout and control cells for panHsp90 (p=0.69) and Hsp70 (p=0.70, Supplementary Fig 5A-D). However, the Hsp90 client proteins GR and GRK2 were significantly decreased in this cell line when compared to control cells (Supplementary Fig 5E and F, H and I, p=0.0034, p=0.0006 respectively). We also studied CHIP, FKBP51 and CypA in the SN56 cells, and similar to the ΔTPR1 mice, CHIP was conspicuously reduced (Supplementary Fig 5E and G, p-0.0034), and CypA was also reduced (Supplementary Fig 5H and K, p=0.0017), whereas FKBP51 was not altered (Supplementary Fig 5H and J, p=0.12), suggesting that the co-chaperone network dysfunction caused by the ΔTPR1 protein resembles loss-of-function of STI1.

Given the disturbed network of Hsp90 binding partners caused by the ΔTPR1 protein, we investigated whether PTVs for these three genes would be tolerated in humans. We found pLI of 0.04, 0.81 and 0.34 for CHIP (*STUB1)*, CypA (*PPIA*) and Pin1 (*PIN1*) respectively, all of which indicate that humans tolerate PTVs in these genes (Fig. 1 and Supplementary Table 1). Also, individual knockout mice of these three genes are viable [36,54,55]. In summary, decreased

levels of ΔTPR1 protein seem to affect chaperone network activity profoundly, leading to a decrease in steady-state levels of several Hsp70/Hsp90 client proteins. This mutant protein also reveals that a group of co-chaperones and Hsp90 accessory proteins are linked to optimal STI1 function.

ΔTPR1 protein causes loss of ES cell self-renewal potential

We surmised that disruption of STI1 activity may affect a number of physiological functions by interfering with the stability of Hsp90 clients. Embryonic development is profoundly affected in STI1 KO mice [2], and our observations in ΔTPR1 mice show they are smaller at birth, potentially suggesting a developmental phenotype. Embryonic stem cells (ESCs) contain abundant levels of chaperone and co-chaperones that may help to maintain critical client proteins involved in stemness [1,56,57]. However, whether STI1 contributes to Hsp90 protection of stem cell clients remains unknown. Therefore, we investigated whether STI1 affects ESCs by generating ESC lines derived from wild-type (WT) and ΔTPR1 homozygous blastocysts. As expected, STI1 levels in ΔTPR1 ESCs dropped markedly when compared with WT cells (Fig 6A, B: $p=0.00015$ and C: $p<0.0001$), and the expected truncated form of 53 kDa was detected (Fig 6C). We investigated the expression of stemness markers in these cell lines by quantifying immunofluorescence images and found a decrease in Sox2 ($p<0.0001$) and Oct4 ($p<0.0001$, Fig 6B). Decreased protein levels detected by immunoblot for Oct4 ($p=0.0012$), Sox2 ($p=0.0025$) and Nanog ($p=0.0148$) confirmed these observations. Hsp90 ($p=0.55$) levels were not affected in ΔTPR1 cells relative to WT controls (Fig 6C-D). Also, mRNA levels were not significantly affected for these markers. Hence, these critical regulators of stemness, Nanog, Sox2 and Oct4, seem to depend on optimal STI1 activity, suggesting that they require Hsp70/Hsp90/STI1 chaperones to maintain their stability.

We next assessed ΔTPR1 and WT ESC colony morphology by staining with alkaline phosphatase (AP), a sensitive and quantitative indicator of undifferentiated stem cells. Although these colonies were almost indistinguishable morphologically, AP revealed a clear difference between cells from ΔTPR1 colonies, which showed a less compact and weaker AP staining pattern with significantly decreased numbers of AP positive cells compared to their control counterparts (Fig 6F and G). Both AP positive colonies and the number of mixed colonies containing AP positive and negative cells differed dramatically between genotypes ($p<0.0001$ and $p=0.039$, respectively). This phenotype was also reported in a STI1 knockdown mESC line [58], providing further evidence that STI1 is important early in development to maintain pluripotency of stem cells.

SSEA1, a surface marker of pluripotency, exhibits a uniform pattern of expression typical of a cell surface protein in ESC colonies from WT mice (Fig 6H). In contrast, SSEA1 in ΔTPR1 ESCs showed an abnormal pattern of distribution (Fig 6H) with a punctuated localization. We detected no changes in mRNA levels for SSEA1 between genotypes (Fig 6I, $p=0.52$). Moreover, flow cytometry analyses revealed a decreased number of cells expressing SSEA1 on the cell surface in ΔTPR1 colonies (Fig 6J), suggesting that trafficking of SSEA1 might be impaired. Hence, not only the levels of potential clients are affected, but also the localization of critical proteins, suggesting multi-leveled requirement for STI1 during development.

To further validate whether STI1 regulates the stemness of ESCs, we assessed their proliferation rate by Ki67 staining and a growth curve. Immunostaining showed that Ki67 positive cells were significantly decreased in ΔTPR1 ESCs as compared to control cells (Fig 7A and B, $p<0.0001$). The growth rate was also reduced in ΔTPR1 ESCs (Fig 7C, Two-Way RM ANOVA $F_{(3,6)}=190.2$, $p<0.0001$), and significantly differed on each day, as revealed by Tukey's post-hoc comparisons

(Day 1, p= 0.002, Day 3, p<0.0001, Day 5, p<0.0001, Day 7, p<0.0001), revealing the involvement of STI1 in the maintenance of self-renewal. Monitoring cellular stress and DNA damage by quantifying the phosphorylation of H2AX, γ-H2AX, revealed elevated numbers of nuclear foci in ΔTPR1 cells (Fig 7D and E, p<0.0001), supporting a function for STI1 in this type of cellular stress response involving DNA damage [2,8]. In summary ESCs expressing hypermorphic STI1 alleles seem to have deficits in proliferation, increased DNA damage and decreased pluripotency capacity.

One way to assess the pluripotency capacity of ESCs is to allow for spontaneous differentiation, by removing LIF from cell media. The differentiating cells form embryonic bodies (EBs) expressing specific markers for the three embryonic germ layers and therefore can provide insight into embryonic development. Both control and ΔTPR1 EBs expressed embryonic germ layer markers (Supplementary Fig 6A and B), confirming their pluripotency capacity. However, WT EB showed Sox2 positive cells, indicating that they still contain undifferentiated cells, whereas ΔTPR1 EB were negative for Sox2 (Fig 7F), suggesting that ΔTPR1 cells might have partially lost their pluripotency, and might be committed for multi-lineage differentiation.

In WT EB cells, STI1 is present in the leading edge of migrating cells (arrows on Fig. 7F, as indicated by nuclei clusters stained with DAPI) and also associates with the cytoskeleton (arrowhead on Fig 7F). In contrast, ΔTPR1 EB cells exhibit preferentially nuclear STI1 (Fig 7F, arrowheads), a phenotype usually observed in cells under increased stress [2,59]. The expression of STI1 was upregulated during spontaneous differentiation to EB formation when compared with undifferentiated ES cells (Fig 7G and H). Statistical analysis revealed significant difference in STI1 levels between differentiated and undifferentiated wild-type EBs (p=0.0286). These data indicate that STI1 may operate as a key regulator of ES cell homeostasis, likely by supporting

the stability of critical proteins involved in ES stemness and regulation. Hence it is likely that abnormal expression of clients and changes in pluripotency in ESCs for ΔTPR1 mice contributed to their reduced size and increased peri-natal lethality.

Cellular homeostasis depends on STI1

The decreased proliferative capacity of stem cells with dysfunctional STI1 suggest the possibility that similar phenotypes may also be observed in differentiated cells. We therefore measured cellular proliferation in MEFs using BrdU. These experiments revealed a decrease of 50% of BrdU positive cells in ΔTPR1 cultures compared with controls (Supplementary Fig 7A and B, $p=0.0004$).

To further test whether STI1 can protect mammalian cells from environmental stress, we examined the survival of control and ΔTPR1 MEFs. In normal conditions, ΔTPR1 cultures showed decreased survival, examined using Live/Dead staining (Supplementary Fig 7C-E). ΔTPR1 cultures included significantly less live cells ($p<0.0001$) and a trend to more dead cells ($p=0.053$). In addition, resilience to oxidative stress in MEFs cultures treated with hydrogen peroxide was assessed by quantifying cleaved caspase-3. ΔTPR1 MEFs appeared to have increased levels of activated caspase, but this did not reach statistical significance (Supplementary Fig 7F and G, $p=0.058$). Overall, although the mutated form of STI1 may be functional under certain conditions, the TPR1 mutant STI1 protein caused global deficits on cellular proliferation and cellular resilience

Hippocampal neuronal loss in aged ΔTPR1 mice

Dysregulation of the Hsp70/Hsp90 chaperone activity has been found in the mammalian nervous system during aging [3,60-62], indicating the untested possibility that a fully functional

chaperone system in mammalian neurons is required for healthy aging. Our cell culture data suggested that complete or partial loss of STI1 function due to the lack of the TPR1 domain decreases cellular resilience. To test whether STI1 activity is required to maintain healthy neuronal aging *in vivo*, we examined hippocampal neurons from ΔTPR1 mice, because these neurons show increased vulnerability to a number of protein misfolding diseases and are also vulnerable during aging [63-66]. To evaluate neuronal resilience in ΔTPR1 mice, we first used silver staining. Silver is increasingly taken up by degenerating neurons, axons or terminals [67-70]. There was no difference between genotypes in silver staining in the Dentate Gyrus of 14-16 months old mice (Fig 8 A and B, p=0.13). However, we detected a significant increase in silver staining in the CA1 region of the hippocampus (Fig 8 C and D, p=0.01), whereas in the CA3 region (Fig 8 E-I) the changes did not reach significance (p=0.12). Nonetheless, we did notice in these images that fields of neurons in each of these CA3 sub-regions (arrows) were severely decreased in older ΔTPR1 mice, suggesting the possibility that at this age the CA3 region was already severely affected and presented neuronal loss.

To determine neuronal survival/viability in ΔTPR1 mice with mutated STI1, we stained the hippocampus of control and ΔTPR1 mice with the marker of mature neurons, NeuN, in 3-5 and 14-16 months old mice and counted neurons in different hippocampal sub-regions. In 3-5 months old mice, there was no reliable loss of CA3 neurons (Fig 9A). Visually and structurally, the neurons of the CA3 pyramidal layer looked similar to those in littermate controls. When the number of neurons was totalled across all subfields of the CA3, (Fig 9A and B), there was no statically significant difference (p=0.068). In contrast, at 14-16 months of age, thinning of the CA3 region was obvious, similar to the silver staining sections. Specifically, the cellular layers in the CA3a and CA3b regions were less densely packed. CA3 pyramidal neurons were more

dispersed compared to control littermates (Fig 9F). Across the whole CA3, there were significantly less neurons in ΔTPR1 mutants compared to controls (Fig 9G, p=0.0003). This decrease in neurons in the CA3 region was the result of reductions in all three sub-regions [CA3a (Fig 9H, p=0.011), CA3b (Fig 9I, p=0.0049) and CA3c (Fig 9J, p=0.0025)].

Numerous studies implicate the CA3 region in spatial memory [65,71-73]. To determine the functional consequence of the age dependent degeneration of hippocampal neurons, we measured performance of mice in the spatial version of the Morris water maze (MWM) task. In the learning/acquisition phase of the task over the four days of training, both controls and ΔTPR1 mice learned to find the target. Animals spent less time each day to get to the target (Two-way Repeated measures ANOVA for Days p<0.0001, and no difference for genotype, p=0.30, Fig 9K) and mice went more directly to target, travelling less distance across the MWM training sessions (Two-way R.M. ANOVA, p<0.0001 for day, no genotype difference p=0.9, Fig 9L). Speed in MWM was comparable between littermate controls and ΔTPR1 mice (p=0.17 R.M Two-way ANOVA, Fig 9M). However, ΔTPR1 mice tended to be less efficient in their travel to the target (p=0.014 at Day 4, R.M. ANOVA). On the fifth day, recall was assessed using a probe trial, in which the platform is removed and we determined how long mice spent in the target quadrant. ΔTPR1 mice showed no preference for the target quadrant when time spent on the target quadrant was compared to time spent in the other quadrants (Fig 9O, p>0.1 for all comparisons), indicating a deficit in memory. In contrast, control mice spent significantly more time in the target quadrant than in the other quadrants. Hence, although ΔTPR1 mice were able to learn the location of the platform they were unable to recall it in the probe trial. In summary, we observed significant degeneration of CA1 and profound loss of CA3 neurons in ΔTPR1 mice that was accompanied by a selective deficit in spatial memory.

DISCUSSION

Our human dataset analyses indicated that some co-chaperones that are not essential in yeast, such as p23 and STI1, are in contrast likely to be essential in humans. We further investigated STI1 function and, in particular, the role of the TPR1 domain in mammals using a new genetically-modified mouse line. RNA-seq data and analysis of client proteins support the notion that STI1 activity regulates client levels by proteostasis rather than at the transcriptome level. We propose that the TPR1 domain of STI1 is required in mammals for efficient STI1 activity. Our findings revealed that STI1 is a master controller of the chaperone network required to maintain the stability of Hsp90 client proteins and several auxiliary co-chaperones.

The role of the TPR1 domain for STI1 co-chaperone activity is not fully comprehended. The TPR1 domain (residues 2-118) is as well conserved (98% identity between human and mouse and 36% identity between human and yeast) as the TPR2B domain (residues 356-477, 99% identity between human and mouse and 39% identity between human and yeast). *C. elegans* STI1 lacks the TPR1 domain, but it is still able to act as a co-chaperone for Hsp70 and Hsp90 [15,74], suggesting the possibility that TPR1 is redundant. Initial work in yeast showed that TPR1 was necessary for activation of GR [19,21], however more recent findings have challenged these results [13,75]. Conversely, the ternary complex formed by Hsp70, Hsp90 and STI1 was less abundant when TPR1 was mutated or deleted [13]. Likewise, yeast expressing human STI1 (Hop) with deleted TPR1 domain or decreased TPR1 activity due to phosphorylation had reduced STI1/Hsp70/Hsp90 ternary complex formation, resulting in weaker activity of GR [13,14]. In yeast, it has been proposed that the two Hsp70 binding domains work cooperatively, with Hsp70 recruitment initially occurring via TPR2B in the absence of Hsp90, which is then shifted to TPR1 in the presence of Hsp90 [14]. The decreased levels of client proteins in

heterozygous ΔTPR1 mice compared to heterozygous STI1 knockout mice support non-redundant roles for mammalian TPR1 and TPR2B *in vivo*.

Our rescue experiment crossing STI1 KO mice with ΔTPR1 mice suggests that the ΔTPR1 protein is at least partially functional during embryonic development. However, heterozygous ΔTPR1 mice present abnormal levels of Hsp90 client proteins, while STI1 heterozygous KO mice do not present such a phenotype. This suggests that *in vivo* the mutated TPR1 protein may somehow compromise chaperone function. Some initial experiments suggested that STI1 may form dimers [19,76-78], but *in vitro* there is evidence that STI1 is a monomer [77]. The mechanisms by which low levels of the ΔTPR1 protein may prevent the wild-type protein function in heterozygous mice *in vivo* are not clear. One possibility is that two STI1 proteins could bind Hsp90 dimers and the ΔTPR1 protein may be less efficient in forming ternary complexes, affecting the wild-type activity. Thus, the mammalian TPR1 domain appears to be required for STI1 regulation of the chaperone machinery, albeit in an incompletely understood way.

STI1 KO mice, SN56 KO cells and ΔTPR1 mouse tissues all show reduced levels of Hsp90 client proteins, such as GRs. In yeast, deletion of STI1 affects GR activity and the v-Src kinase conformation, but GR levels are unaffected [79]. Also, other yeast Hsp90 clients were not affected by elimination of STI1 [79]. In contrast, in mice we found that the levels of a number of known Hsp90 client proteins, such as GR, Tau, GRK2, Nanog, Sox2 and Oct4, were all dependent on STI1. These differences between mammalian and yeast STI1 in client specificity highlight the increased dependence on proteostasis regulation and STI1 activity in mammalian cells.

Our results also reveal that accessory proteins with PPIase activity as well as the E3 ligase CHIP are significantly reduced in ΔTPR1 mouse tissues and in STI1 SN56 KO cells. In contrast, other key proteins involved in the heat shock response, such as HSF1, Hsp40, Hsp70 and Hsp90 are not affected by expression of the ΔTPR1 protein. These results suggest that some of these accessory proteins may also require fully functional Hsp70/Hsp90 cycles to maintain their levels, supporting the notion that STI1 acts as a regulatory node for the chaperone machinery and that it is important both for recruiting client proteins and for stabilizing certain co-chaperones, allowing them to regulate different steps of the chaperone cycle.

Pluripotency genes, such as Sox2, Oct4 and Nanog have been proposed to be clients of Hsp90 [1]. Our results confirm and extend these observations by demonstrating marked changes in the pluripotency capacity of ΔTPR1 ESCs, with downregulation of key pluripotency factors, and loss of alkaline phosphatase activity, which may contribute to the abnormal development of mutant mice. Growing evidence reveals that pluripotent cells exhibit enhanced mechanisms of proteostasis in order to maintain their immortality and control cell fate decisions. The chaperone machinery is suggested to play an important role in this regulation [80,81]. The levels of specific chaperones can be determinant for ES cell function and Hsp90 inhibition or silencing lead to cell differentiation, indicating a role for chaperones in stemness maintenance [1]. Indeed, ESCs are sensitive to manipulations of proteostasis and a slight proteasome inhibition can affect the pluripotency status and cell survival due to accumulation of damaged proteins [82]. Our findings support a role for STI1 in the proteostasis of ES cells and reveal proteins involved in the maintenance of pluripotency status as clients of Hsp70/Hsp90/STI1. Whether the abnormal embryonic development we observed here can contribute to life-long phenotypes, influencing for

example metabolism, needs to be further explored by using conditional and inducible STI1 elimination.

Previous work has shown that chaperone networks can be dysregulated with age, and changes in chaperone levels in *C. elegans* can affect phenotypes due to protein misfolding [3,15,21]. In *C. elegans*, KO of STI1 reduces lifespan as well [15]. However, whether mammalian neurons require STI1 mediated activity for healthy aging *in vivo* is, to the best of our knowledge, unknown. The CA3 hippocampal region is particularly vulnerable in stress [83,84] and disease [63,84]. CA3 neurons support spatial memory [85] due to their excitatory and modifiable connections with the Dentate Gyrus and CA1 regions of the hippocampus. Damage to the CA3 region has been shown to produce deficits in spatial memory [65,72,73]. We found that hippocampal neurons in the CA1 region show increased features related to degeneration. However, most remarkably, we found a pronounced age-dependent loss of CA3 neurons. In agreement with the loss of CA3 neurons in ΔTPR1 mice, we find that in ΔTPR1 mice spatial learning does not seem to be affected, whereas memory recall is severely compromised.

The mechanism by which abnormal STI1 activity afects neurons and whether other brain regions show increased susceptibility to decreased STI1 activity needs to be further explored. Certainly, the increased susceptibility to stress in STI1-deficient cells may contribute to the abnormal loss of CA3 neurons during aging. Moreover, the profound and widespread alteration in Hsp90 client proteins, which are known to contribute to neuronal function, may also be relevant for neuronal aging. However, whether these effects of STI1 in neurons are cell autonomous or non-cell autonomous will need to be investigated [86]. Future experiments using conditional approaches to mutate STI1 in neurons or glia are warranted to explore these mechanisms.

Cancer cells and senescent cells seem to be particularly reliant on Hsp90 activity to maintain proteostasis for survival [87]. Indeed, Hsp90 inhibitors are currently being tested in different cancer types [88]. Moreover, recent experiments have shown that partial inhibition of the Hsp90 system can increase life span in a mouse model of aging, by killing cells that have senescent phenotype that contribute to overall organism inflammation and stress [89]. Our experiments demonstrated that STI1 might be exploited as a key inhibitor of the Hsp90 system to influence a host of client proteins in mammals and could be used to modulate Hsp90 activity efficiently. Overall, it will be critical to find a balance between chaperone network activity that allows neurons to cope with increased stress of aging and still allow for proper disposal of damaged or senescent cells. The ΔTPR1 domain seems to be required for optimal STI1 activity *in vivo* and the consequences of decreased STI1 function are widespread at the organism level. Notably, these results illuminate a requirement for optimal STI1 activity to maintain healthy hippocampal aging in mammals. In conclusion, the use of hypomorphic alleles of essential co-chaperones may provide new insight on the roles of these critical proteins in mammalian physiology, extending their functions learned initially in organisms that are more distant from humans.

MATERIALS AND METHODS

Analysis of Hsp90 and co-chaperone variants in human datasets

To address the importance of genetic variants in chaperone networks in humans, we evaluated the frequency of loss-of-function variants (protein truncating variants, PTVs) in multiple large datasets aggregating human genetic information. Specifically, we sought PTVs in the following genes: *STI1*, *HSP90AA1*, *HSP90AB1*, *PTGES3*, *AHSA1*, *FKBP5*, *PIN1*, *STUB1*, *CDC37*, *PPIA*, *PPP5C*, and *SGTA*. To assess the frequency of PTVs in these genes in a large and ethnically diverse cohort of relatively healthy individuals, and to extract the probability of loss-of-function (pLI) score for each gene, we used the Exome Aggregation Consortium (ExAC, n=60,706) and the Genome Aggregation Database (gnomAD, n=138,632), [22,90]. Due to the difficulty in sequencing regions of *HSPA1A* (Hsp70), an accurate pLI score was not obtained. Next, we assessed the frequency of PTVs, missense variants, insertions, deletions, and/or duplications in these genes of interest in a cohort of clinically-ascertained individuals. To this end, we used the GWAS Catalog, ClinVar, and DatabasE of genomiC varIation and Phenotype in Humans using Ensembl Resources (DECIPHER) [91-96]. We did not use the Human Gene Mutation Database (HGMD) as this resource is no longer open-source, and currently only provides minimal information for variants identified in patients. We applied the following criteria to ensure that PTVs observed are likely to be true PTVs: 1) ensuring the PTV is present in the canonical transcript; 2) the PTV occurs prior to the last exon of the gene; and 3) the site and the surrounding region of the PTV are sufficiently covered, there is adequate allele balance between the reference allele and the alternate allele for heterozygous PTVs, and the variant does not display strand bias. For variation reported by ClinVar and DECIPHER, we only included information on cases with single nucleotide variants (SNVs), small insertions or deletions

(indels), or copy number variation (CNV, gain and loss) of large genomic regions, that were classified as either ‘pathogenic’ or ‘likely pathogenic’ by each database’s respective criteria.

Mouse line generation

We used Cre/loxP technology to generate mice expressing *Stip1* lacking the TPR1 domain (ΔTPR1-STI1). Genetically-modified mice were generated by Ozgene (Perth, Australia) on a C57BL/6J ES genetic background using standard homologous recombination techniques. In short, a FRT-flanked PGK-neomycin cassette was inserted upstream of exon 2. LoxP sites were inserted upstream of the selection cassette and downstream of exon 3. The construct was electroporated into embryonic stem (ES) cells from C57BL/6J mice and targeted ES cells were injected into C57BL/6J blastocysts. Chimeric mice obtained were crossed to C57BL/6J mice to generate STI1-flox mice. To remove the selection cassette, STI1-flox mice were crossed to OzFlpE, a knock-in line that contains the *FlpE* variant of the *Saccharomyces cerevisiae FLP1* recombinase at the *Rosa26* locus, followed by backcrossing to C57BL/6J to remove *FlpE*. The ΔTPR1-STI1 mice were obtained by crossing STI1-flox to OzCre mice (PGK-Cre at the *Rosa26* locus), which allowed for germline deletion of exons 2 and 3. Further breeding allowed the removal of the Cre transgene. We confirmed the recombination of the *Stip1 locus* by genome sequencing (not shown). After recombination, we confirmed that the translation initiation codon of the mutated mRNA lacks the neighboring Kozak consensus [97], which likely contributed to less efficient translation of ΔTPR1-STI1 protein.

Ethics Statement

Animals were housed and maintained at The University of Western Ontario by the Animal Care and Veterinary Service. Animals were used as outlined in our Animal Use Protocols (2016-103; 2016-104), which adhered to the Canadian Council of Animal Care (CCAC) guidelines. Animals were housed with 3-4 littermates/cage, and had *ad libitum* access to food (Harlan) and water in standard plexiglass cages in a room with light/dark cycle from 7am-7pm in temperature and humidity-controlled rooms (22-25°C, with 40-60% humidity). Animals were regularly monitored by Animal Care and Veterinary Services Staff and by the researchers and technicians in the lab.

Mouse embryonic fibroblast (MEF) culture

MEF cultures were generated as previously described [2,98]. Heterozygous breeding pairs were used and E13.5 embryos were collected and isolated for culture, with 3-5 embryos/genotype being collected for each experiment. Embryos were dissected in Hanks Balanced Salt Solution on ice. Head and liver were excluded and all other tissues were used to generate MEF cultures. Cultures were grown in 10% FBS (Gibco), 1% L-Glu, 1% penicillin-streptomycin in DMEM. Media was changed every 3-4 days or as required. MEFs were grown for several passages and frozen at passage 2 (P2), P3, P4 and P6. Western blotting and q-PCR were performed on P4 MEFs, to guarantee that maternal STI1 was not affecting growth and patterns of protein expression [2]. 2 x 10^6 cells/mL were frozen in 10% DMSO, 20% FBS in DMEM for 24 hours at -80°C, then transferred to liquid nitrogen for long-term storage. Before their use for experiments, MEFs were thawed and plated in T25 flasks in media with 20% FBS, allowed to reach 70-80% confluency, then split to smaller plates in normal medium, as required.

Embryonic stem cells derivation

Mouse embryonic stem cells (mESC) were derived from late blastocyst stage (obtained from ΔTPR1 heterozygous mating) using Leukemia inhibitory factor (LIF) and two inhibitors of signaling pathways, ERK (PD032901, Sigma) and GSK3 (CHIR99021, Sigma), in order to maintain cells undifferentiated during the derivation process [99]. The cells were cultured in GMEM (Sigma) supplemented with 15% FBS (Qualified, Gibco), 1X Pen Strep, 2 mM GlutaMAX, 1 mM sodium pyruvate, 0.1 mM MEM NEAA (Invitrogen), 0.1 mM 2-Mercaptoethanol (Gibco), 10^3 IU LIF.

CRISPR/Cas9 generation of STI1 SN56 KO cells

The guide RNAs for the mouse STIP1 gene (STI1 Top 1: 5'CACCGGTAGTCTCCTTTCTTGGCGT 3' and STI1 Bottom 1 5'AAACACGCCAAGAAAGGAGACTACC 3') were designed using Optimized CRISPR Design (http://crispr.mit.edu/). They were phosphorylated, annealed and cloned at BbsI enzyme restriction site into the px330 modified vector (Addgene) [100], according to instructions from Addgene. The construct was sequenced and used to transfect SN56 cells with Lipofectamine 2000 (Invitrogen). Clones were then isolated by serial dilution. Isolated clones were grown separately. Immunoblot analysis was used to determine clones showing complete STI1 KO. Although several clones were obtained with decreased levels of STI1, only one clone showed completely eliminated STI1 protein expression and this clone was expanded and used to further investigate Hsp90 client proteins and co-chaperones.

In vitro differentiation of mESC

Cells were harvested by trypsinization and cultured in petri dishes in embryonic stem cell medium (described above) without LIF to allow embryoid body (aggregated cells) formation.

After 4 days in culture, embryoid bodies (EB) were plated onto gelatin-coated Ibidi dishes (Ibidi) followed by 72 hours of incubation. The potential of EBs to differentiate into three embryonic germ layers was assessed by staining with anti-α-smooth muscle actin antibody (1:100, Catalog# MAB1420, Mouse mAb Novus Biologicals, mesoderm marker), anti-α-fetoprotein polyclonal antibody (1:100, Catalog# AF1369, Goat pAb, R&D, endoderm marker) or anti-βIII tubulin monoclonal antibody (1:100, Catalog# MAB1195, Mouse mAb, R&D, ectoderm marker).

Alkaline phosphatase assay

ES cells plated on gelatin-coated coverslips were cultured for 72 hours in complete medium (described above) and stained using the Alkaline Phosphatase Staining Kit (Stemgent) according to manufacturer's instructions. Alkaline phosphatase staining is more abundant in undifferentiated ESCs and allows for visualization of cell morphology. The positive, negative and mixed colonies for AP staining were quantified using Image J software.

Quantitative RT-PCR

RNA was isolated using the Aurum Total RNA Fatty and Fibrous Tissue Pack (Cat# 732-6870) Bio-Rad kit according to the manufacturer's instructions. cDNA was synthesized using 2 µg RNA according to protocol (Applied Biosystems). DNA was diluted and qPCR performed using SYBR Green, on a Bio-Rad CFX96 thermocycler. qRT–PCR analysis for mESCs was performed in biological and technical triplicates. GAPDH was used as reference gene for data normalization. Primer pairs used were as follows (Sigma): Nanog-F: AAGGATGAAGTGCAAGCGGT, Nanog-R: GGTGCTGAGCCCTTCTGAATC, Oct4-F: AGCACGAGTGGAAAGCAACT, Oct4-R: TCATGTCCTGGGACTCCTCG, Sox2-F: GCTCGCAGACCTACATGAAC, Sox2-R: GCCTCGGACTTGACCACAG, Klf4-F:

AGAACAGCCACCCACACTTG, SSEA1-F: CGGACCGACTCGGATGTCT, SSEA1-R: TTGGATCGCTCCTGGAATAGA, GAPDH-F: CCCCAATCTCCGTCGTG, GAPDH-R: GCCTGCTTCACCACCTTCT.

Cortices from 14-16 months old perfused male mice were dissected on ice and then frozen on dry ice before transfer to -80°C. Samples were homogenized in TRIzol and RNA was isolated using the Aurum Total RNA for fatty and fibrous tissue kit and cDNA was generated, as described in Beraldo et al. [2]. β-actin was used to normalize mRNA levels and negative controls were included with four to five separate animal tissue extracts per genotype as biological replicates on each plate. The following primers were used to assess mRNA levels. STI1-F: 5'-GCCAAGAAAGGAGACTACCAG-3' and STI1-R: 5'- TCATAGGTTCGTTTGGCTTCC-3'for exons 2 and 3 and STI1-97F: ACCCCAGATGTGCTCAAGAA and STI1-97R: TCTCCTCCAAAGCCAAGTCA for exons 8 and 9. Hsp90α-F:CCACCCTGCTCTGTACTACT; Hsp90α- R:CCAGGGCA TCTGAAGCATTA; Hsp90β-F: CTCGGCTTTCCCGTCAAGAT, Hsp90β-R: GTCCAGGGCATCTGAAGCAT, Hsp70-R: ACCTTGACAGTAATCGGTGC, Hsp70-F: CTCCCGGTGTGGTCTAGAAA, HSF1-F: GATGACACCGAGTTCCAGCA, HSF1-R: CACTCTTCAGGGTGGACACG, CHIP-F: CTTCTACCCTCAATTCCGCCT, CHIP-R: CATTGAGAAGTGGCCTTCCGA, Pin1-177F: AAGCAGACGCTCCATACCTG, Pin1-177R: AGAGTCTGGACACGTGGGTA, Fkbp5-83F: CTGCTGTGGTGGAAGGACAT, Fkbp5-83R: TCCCAATCGGAATGTCGTGG, Nr3c1-160F: TGTGAGTTCTCCTCCGTCCA, Nr3c1-160R: GTAATTGTGCTGTCCTTCCACTG, Mapt-200F: AACCAGTATGGCTGACCCTC,

Mapt-200R: TCACGTCTTCAGCAGTTGGA, Grk2-119F: CTGCCAGAGCCCAGCATC,

Grk2-119R: AGGCAGAAGTCCCGGAAAAG, Actin-F: TGGAATCCTGTGGCATCCATGA, Actin-R: AATGCCTGGGTACATGGTGGTA.

Growth curve assay

mESCs ($2x10^4$ cells) were plated in 24 well dishes and the total cell number was counted every 48h using a Neubauer chamber. Cells were counted in triplicate cultures by an experimenter blind to the genotypes. The experiment was repeated twice.

Flow cytometry analysis

Cells ($1 x10^6$) harvested by trypsinization were incubated with 5% BSA in PBS for 30 min a 4ºC. The primary antibody (1:100, anti-SSEA1, Catalog# 4744, Mouse mAb, Cell Signaling) was incubated in 1% BSA in PBS for 30 min a 4ºC. Mouse Alexa 488 (1:200, Goat-anti-Mouse, Catalog# R37120, Molecular Probes) was used as a secondary antibody. Flow cytometry analysis was performed at London Regional Flow Cytometry Facility (LRFCF) at Robarts Research Institute using a FACSCalibur (Becton Dickson – BD – Biosciences). Data were generated using FlowJo v9 (FlowJo, LLC).

Immunofluorescence

Immunofluorescence labelling of cell cultures was conducted as previously described [2]. For MEFs, P4 cells were used. Cells were split onto 24-well dishes onto poly-lysine coated coverslips at a density of $6 x 10^4$ cells. Once MEFs reached 80% confluence (~2-4 days), media was removed, coverslips were washed three times with PBS and then fixed for 20 minutes with 4% cold paraformaldehyde (PFA). After three PBS 0.5% Triton X-100 washes, cells were blocked in 0.5% Triton X-100 and 5% bovine serum albumin (BSA) in PBS for one hour at room temperature (RT) before overnight incubation with primary antibodies in 0.1% Triton X-100 and

0.1% BSA in PBS at 4°C. Cells were incubated with STI1 antibody (1:200 in-house antibody generated by Bethyl Laboratories Montgomery, USA using recombinant STI1), anti-Hsp70 (1:100, Catalog# Ab2787, Mouse mAb, Abcam), anti-Hsp90 (1:50, Catalog# 4877, Rabbit mAb, Cell Signalling), Cell Signalling Cleaved-caspase 3 (1:400, Catalog# 9664, Rabbit mAb, Cell Signalling). For mESC the following antibodies were used: anti-βIII-Tubulin (1:100, Catalog# MAB1195, Mouse mAb, R&D, ectoderm marker), anti-STI1 (1:400-(in-house antibody generated by Bethyl Laboratories Montgomery, USA) (Beraldo et al., 2013), anti-Oct3/4 (1:200, Catalog# sc-5279, Mouse mAb Santa Cruz), anti-Sox2 (1:200, Catalog# 14-9811-82, Thermo Fisher, Rat mAb), anti-Nanog (1:200, Catalog# 8822, Rabbit mAb, Cell Signaling), anti-SSEA-1 (1:200, Catalog# 4744, Mouse mAb, Cell Signaling), phospho-H2AX (1:200, Catalog #9718, Rabbit mAb, Cell Signaling), Ki67 (1:100, Catalog# ab16667, Rabbit mAb, Abcam). Alexa Fluor-conjugated secondary antibodies (Molecular probes) were used at 1:800 in 0.5% bovine serum albumin and 0.1% Triton X-100 in PBS. Cells were counterstained with DAPI, mounted onto slides using Immu-Mount (Thermo Scientific) and imaged using Leica TCS SP8 (Leica Microsystems Inc., Ontario, Canada) confocal system (63X objective, N.A. of 1.4 and 40X objective, N.A. of 1.3). For immunofluorescent labelling in cells, 2-3 coverslips per embryo were imaged and 8 random fields of view were captured for each coverslip by a researcher blind to genotypes.

RNA-seq analysis

For mRNA sequencing 5 STI1 wt/wt and 5 STI1 dTPR/dTPR samples were used. RNA quality was determined with RNA 2100 Bioanalyzer (Agilent), and samples with RIN values ranged between 8.2 and 8.7 were used. Sequencing-compatible poly(A)-terminated single-end libraries were generated using an RNA Library prep kit (SENSE Total RNA-Seq Library Prep Kit, 009;

Lexogen) following manufacturer's instructions. Libraries were barcoded and sequenced on a NextSeq Series Sequencing System (HUJI Center for Genomic Technologies) using Illumina flow cell (Illumina 500 NextSeq High Output v2 Kit, FC-404-2005; Illumina). The sequencing data were uploaded to the usegalaxy.org [101] web platform for further analysis. All reads were aligned to the mouse reference genome (GRCm38/mm10) with an average 93.7% mapping (TopHat2) [102]. Gene expression counts were generated using HTseq-count [103] (GRCm38/mm10) and expression analysis was performed using the Bioconductor DESeq2 [104] software via R platform [105]. Libraries from all samples were overall similar in depth.

Cell death and viability assay

Cell death was assessed by the Live/Dead^{TM} Viability/Cytotoxicity Kit assay for mammalian cells (Thermo Fisher Scientific – Invitrogen – Cat# L3224) as previously described [2,59,106]. Briefly, SN56 cells and P4 MEFs were incubated with the calcein-AM/ethidium homodimer mix according to the manufacturer's instructions in the original medium for 45 min and then washed 3 times with Krebs-Ringer HEPES (KRH) buffer. Images were collected using the LSM 510 META ConfoCor2 equipped with a 10x/0.3 objective. 488 nm laser was used to detect for calcein (live cells) or ethidium homodimer (dead cells). Cell death levels were quantified as the percentage of dead cells relative to the total number of cells. The numbers of live and dead cells were quantified, with 4-5 embryos per genotype and each embryo in duplicate or triplicate. Eight randomized fields of view were analysed.

BrdU proliferation assay

BrdU proliferation assay was performed as described previously [2]. P4 MEFs were serum starved for 24 h before 30 µM BrdU in sterile water was added to culture media for 1.5 h. Media

was removed and cells were fixed with cold 4% PFA for 20 minutes. Cells were washed with PBS 3 times then treated with 2 M HCl for 30 minutes. Acid was quickly removed and 9.1 M Sodium Borate was added to cells for 12 minutes. Cells were then washed with PBS three times, blocked for 1 h in PBS + 0.3% Triton X-100 and 5% normal goat serum, and then incubated overnight at 4°C with anti-BrdU biotin conjugate (1:100, Catalog# MAB3262B, Millipore), followed by incubation with Streptavidin Alexa Fluor 488 conjugate (1:800, Catalog# S32354, Invitrogen). Cells were washed with PBS then treated for 20 minutes with Hoechst. The BrdU positive nuclei were quantified and compared to total nuclei, with 4-5 embryos per genotype. Experiments were replicated three times. Experimenter was blind during image capture.

Oxidative stress in MEFs

P4 MEFs were serum starved for 48 h before treatment with 150 µM H_2O_2 for 3 h. After incubation, media was removed and cells were fixed with cold 4% PFA and cleaved caspase-3 was immune-fluorescently detected (1:400, Catalog# 9661, Rabbit mAb, Cell Signalling). Cells positive for cleaved caspase-3 were quantified as compared to total nuclei. Two-three coverslips/embryo were imaged using Zeiss Axiovert 100 Apotome at 10X magnification (N.A. of 0.3), with 8 random fields of view being captured. Experimenter was blind during imaging and fluorescence changes were calculated and averaged for each embryo (4 per genotype).

Expression of STI1 recombinant domains in bacteria

Expression of recombinant STI1 and analysis of antibody interaction was performed as previously described [107].

Western Blotting

Mice were decapitated and brains were rapidly excised on ice. Brains were dissected into cortex and hippocampus on ice and flash frozen on dry ice before transfer to -80°C. Protein extraction and Western blot were carried out as previously described [2,108]. Briefly, protein was extracted from whole cell lysates and brain tissue using ice cold RIPA lysis buffer with protease and phosphatase inhibitors. Samples were centrifuged for 20 minutes at 10,000 g at 4°C, then supernatant was collected and used for quantifying protein concentration using the Bio-Rad DC Protein assay. 5-30 µg of protein was loaded on Bolt 4-12% Bis-Tris gradient gels. The primary antibodies used in immunoblotting were: anti-STI1 (1:5000, in-house antibody generated by Bethyl Laboratories Montgomery, USA) [2], anti-Hsp90 (1:1000, Catalog# 4877, Rabbit mAb, Cell Signalling), anti-Hsp70 (1:1000, Catalog# ab2787, Abcam), anti-Hsp40 (1:1000, Catalog# 4868, Rabbit mAb, Cell Signalling) anti-CHIP (1:1000, Catalog# 2080, Rabbit mAb, Cell Signalling), anti-Glucocorticoid Receptor (1:1000, Catalog# 3660, Rabbit mAb, Cell Signalling), anti-HSF1 (1:1000, Catalog# 4356, Cell Signalling), anti-Hsp90β (1:1000, Catalog# 5087, Rabbit pAb, Cell Signalling), anti-GRK2 (1:1000 Catalog# 3982, Rabbit pAb, Cell Signalling) anti-FKBP51 (1:1000, ab2901, Rabbit pAb, Abcam), anti-PrP 8H4 (1:2000, Catalog# ab61409, Mouse mAb, Abcam); anti-CypA (1:2000, Catalog# ab126738, Rabbit mAb, Abcam), anti-tau H150 (1:200, Catalog# sc-5587, Rabbit pAb); anti-Pin1 (1:250, Catalog# sc-15340, Rabbit pAb, Santa Cruz) anti-Oct3/4 (Catalog# sc-5279, Mouse mAb Santa Cruz), anti-Sox2 (1:200, Catalog# MA1-014, Thermo Fisher, Mouse mAb), anti-Nanog (1:200, Catalog# 8822, Rabbit mAb, Cell Signalling). Protein expression, relative to actin and normalized to WT controls was quantified using the Alpha Innotech software for the FluoroChemQ chemiluminescent exposure system (Alpha Innotech; GE Healthcare, London, ON, Canada) or ImageLab for ChemiDoc system

(BioRad). At least 2 independent blots were repeated with no less than four animals analyzed for each protein (generally n=4-9).

Silver Staining

Silver staining was performed as described previously [67]. Briefly, after trans-cardial perfusion, mouse brains were fixed in 4% PFA for 48 h before long-term storage in PBS + 0.02% sodium azide. Brains were cut using Leica VT1000S Vibratome, at 30 µm thickness, sections were stored in PBS + 0.02% sodium azide. Using 6-well plates and net-wells, free-floating sections were stained with the NeuroSilverTM staining kit II (FD NeuroTechnologies, Inc., Baltimore, USA) following manufacturer's instructions. This kit labels degenerating neuronal bodies, processes and terminals. Images were taken using Zeiss Axioskop Optical Microscope at 20X magnification, with two images being taken along the dentate gyrus, from the apex to the hilus/opening of the blades, three images of the CA3, respective to CA3 subfields (CA3a, CA3b, CA3c), and one image from the CA1 region. At least 4 sections from 4 animals/genotype were stained and sections selected were at least 120 µm apart. Using ImageJ (Fiji) Software (NIH), images were converted to 8 bits and thresholded to make the silver particles black and background white (Circularity of 0-0.65). Particles were numbered and averaged for each animal. The same parameters were used for each section, animal and both genotypes.

NeuN Staining and Hippocampal Neuron Density

NeuN staining was performed as described previously [67]. Briefly, 30 µm thick sections were mounted onto charged microscope slides, boiled in 10 mM sodium citrate for 20 minutes and then cooled for 40 minutes to room temperature for antigen retrieval. Sections were then washed three times in water, then immersed in 3% hydrogen peroxide for 10 minutes, followed by two

washes in 0.025% Triton-X PBS. Tissue was blocked in 10% normal goat serum and 1% BSA in PBS for 2 h, at RT. Sections were incubated with anti-NeuN (1:15000, Catalog# ab104224, Mouse mAb, Abcam) overnight at 4°C, washed twice with 0.025% Triton-X in PBS, then incubated for 1 h in biotinylated goat anti-mouse secondary antibody (1:200, Catalog# BA9200, Vector Laboratories). Following washes, sections were incubated for 30 minutes in Vectastain Elite ABC Kit (Catalog# PK-6100, Vector Laboratories) following manufacturer's instructions. Next, sections were treated with DAB Peroxidase Substrate Kit (Catalog# SK-4100, Vector Laboratories) following manufacturer's instructions. Sections were re-washed, then dehydrated and cleared using a series of ethanol and xylene washes. Staining was performed in 3-5 months old and 14-16 months old mice. Four sections at least 60 µm apart were selected from each animal to allow for unbiased selection within similar coordinates for each animal, starting around Lateral 2.356 mm (sagittal sections). Images were taken using Zeiss Axioskop Optical Microscope at 20X magnification. For each section, one image of each subfield of the CA3 region of the hippocampus was taken (CA3a, CA3b, CA3c). The number of NeuN cells in each subfield of the CA3 was counted, in each section and averaged per animal. The number of NeuN positive cells was then averaged across four to five animals, per genotype. By adding the number of cells across each CA3 subfield, the average sum of neurons in the CA3 was also quantified. The experimenter was blind to genotypes during imaging and quantification.

Morris Water Maze (MWM)

The spatial version of the MWM was performed as described elsewhere [34,67,109]. Nine-ten animals/genotype were used in MWM based on previous estimates using this protocol [34,67,109] and tested mice were 9 months of age. Animals were allowed to acclimatize to the room for 30-40 minutes before the start of the experiment. Experiments were performed in a 22-

24°C room and mice were placed in a 1.5 m diameter pool (water temperature was 26°C) with a transparent plastic platform 1 cm below water surface. Two large lamps next to the pool were lit all throughout the experiment and spatial cues were present on the walls. Mice were counterbalanced and trained over four days to find a platform in one quadrant of the water maze. Animals had four training sessions per day lasting 90 s each (with a 15 min inter-trial interval). If a mouse failed to reach the platform it was positioned on it for 10 seconds before being removed from the pool. In analysis, a 60 s latency to reach platform value was input for animals that exceeded 60 s before reaching the platform and ending the trial. On the fifth day, mice were placed in the pool once (without the platform) for 60 s. Time spent in target quadrant was compared to other quadrants. Activity and behaviour was recorded with ANY-Maze Software. The researcher was not blind to genotypes during experiments, and animals were randomly allocated as for the order they did the task. Target quadrant and analysis was blind.

Statistical Analyses

Data were compiled and analyzed using GraphPad Prism 6.0 Software and results are represented as Mean ± SEM. Comparison of two groups was analyzed using Student's t-test (two sided). For groups larger than two, One or Two-Way ANOVA or Repeated Measures Two-Way ANOVA was used when needed and Post-hoc tests corrected for multiple comparisons was used when required. Mouse birth frequencies were analysed by the Chi-Square test.

Author contributions: Designed experiments, performed experiments and analysed data: REL, MHL, AR, GM, FHB, AM, RG; Performed experiments and analysed data: JF; Analysed data: SMKF, W-YC, DG; Contributed with reagents and special tools: VRM, MLD; Designed

experiments: HS, VFP, MAMP; Wrote manuscript: REL, MHL, SMKF, VFP, HS, MAMP. All authors edited and approved the final version of the manuscript.

Acknowledgements:

We thank Jose Marques-Lopes for help in generating MEFs. MAMP and VFP received support from the Canadian Institutes of Health Research (MOP 126000, MOP 136930, MOP 89919), National Science and Engineering Research Council of Canada (402524-2013 RGPIN). MAMP, MLD and FB received support from the ALS Canada. Initial generation of STI1 mutant mice was supported by PrioNet-Canada and FAPESP (Brazil) to MAMP, VFP and VRM. MHL received a FAPESP Sabbatical fellowship (2016/00440-9) and a research grant (2017/20271-0). HS acknowledges support by The Israeli Ministry of Science, Technology and Space, Grant No. 53140, The Israel I-Core Center of Excellence for Mass Trauma, the Legacy Heritage Science Initiative (LHSI) of The Israel Science Foundation Grant No. 817/13, and the Edmond and Lily Safra Center for Brain Sciences (ELSC). REL received support from OGS. SMKF is supported by the ALS Canada Tim E. Noël Postdoctoral Fellowship.

Figure Legends:

Figure 1: *STIP1* interactions A. RCircos image showing human chromosome ideogram displaying *STIP1*, *HSP90AA1*, *HSP90AB1*, *PTGES3*, *AHSA1*, *FKBP5*, *PIN1*, *STUB1*, *CDC37*, *PPIA*, *PPP5C*, and *SGTA*. The physical interactions among them are shown by pink ribbons. **B.** Functional and physical interactions of genes of interest (highlighted in outer red circles). **C.** Functional and physical interactions of STIP1. A pink connection indicates a physical interaction between genes; gene co-expression is purple; a blue connection indicates shared pathways between genes; and genes with shared protein domains is displayed by a yellow connection. Interactions were created in GeneMANIA with slight modifications.

Figure 2: Generation and characterization of ΔTPR1 mice

A. Simplified scheme of the *Stip1* gene locus with or without recombination to remove exons 2 and 3. **B.** Scheme of major domains of the STI1 protein with or without the TPR1 domain (143 amino acid deletion). **C.** Picture of 3 week old homozygous ΔTPR1 mice (star) and littermate controls. **D.** Comparison of body weights of mice from 1-70 weeks of age (open circle for WT and dark triangle for ΔTPR1 mice). N=7-10 mice for each time point. Data analyzed using Two-Way ANOVA, multiple comparisons corrected with Sidak's test. **E-G.** Different physiological parameters obtained using metabolic cages during 24 h recordings for WT (clear bars) and ΔTPR1 mice (black bars). Data are mean ±SEM (N=8). **H.** Analysis of adult cortical brain tissue STI1 transcripts using primers for exons 2 and 3. **I.** qPCR analysis for STI1 transcripts using primers for exons 8 and 9 (N=8). **J.** Hsp90β mRNA expression in adult cortical brain tissue. **K.** Hsp70 mRNA expression in adult cortical brain tissue. (N=4) **L.** Representative *Western* blots of STI1 expression in adult cortical brain extracts. Arrow full-length STI1, arrowhead ΔTPR1 protein. **M.** Quantitative analysis of STI1 levels in WT (white bar), ΔTPR1 heterozygous (HET) for full length STI1 (66 kDa, light grey bar) and truncated protein (53 kDa, dark grey bar with stripes) and homozygous ΔTPR1 mice (black bar). Data are mean ±SEM (N=8). One-way ANOVA with corrections for multiple comparisons with Dunnett's test. **N.** Representative *Western* Blots for Hsp90 and Hsp70 expression in male adult mice (N=4/genotype). O-Q Quantification of Hsp90 or Hsp70 protein levels in WT, HET and ΔTPR1 tissue. Data are mean ±SEM (*$p<0.05$, **$p<0.001$, ***$p<0.0001$).

Figure 3. Normal levels of HSF1, Hsp40 and FKBP51 in ΔTPR1 mouse brain.

A. Representative immunoblots for Heat Shock Factor 1 (HSF1) and Hsp40 levels in cortical extracts. **B**. and **C.** Densitometric quantification of protein levels (N=4/genotype). **D.** Representative immunoblot for FKBP51 in WT and ΔTPR1 male adult cortical extracts. **E.** Quantification of protein levels of D. (N=5/genotype).

Figure 4. Disturbed chaperone network protein levels and client proteins in ΔTPR1 mouse brain.

A. Representative immunoblots for glucocorticoid receptor, STI1, total Tau, G-coupled receptor kinase 2 (GRK2) and actin loading control in male brain lysates. **B.** Quantification of glucocorticoid receptor levels (N=8/genotype). **C.** Quantification of total tau levels (N=4/genotype). **D.** Quantification of GRK2 levels in cortical brain homogenates (N=4/genotype). Data are Mean ± S.E.M. *p<0.05, **p<0.01, *** p<0.0001. **E.** Representative immunoblots probing for the levels of STI1, CHIP, Pin1 and Cyclophilin A (CypA) in adult brain cortical lysates. **F** & **G** Quantification of CHIP and Pin1 levels (N=8 for WT and ΔTPR1 and N=4 for HET for CHIP and N=8 for all genotypes for Pin1). **H.** Quantification of CypA levels. (N=4). (n=4/genotype). All data are Mean ± S.E.M. *p<0.05, **p<0.01, *** p<0.0001.

Figure 5. Levels of client proteins and co-chaperones in STI1 knockout mice.

A. Representative immunoblot for Glucocorticoid receptor, STI1, Tau and Actin (loading control) in wild-type (WT) and heterozygous STI1 knockout (STKO-HET) adult mouse cortical extracts. **B.** & **C.** Quantification of glucocorticoid receptor and Tau levels (N=4). **D.** Representative immunoblots for STI1, FKBP51, Pin1, CHIP and Actin (loading control) in adult mouse cortical extracts. **E-H.** Quantification of STI1, FKBP51, Pin1 and CHIP protein levels. (N=4/genotype). All data are Mean ± S.E.M. *p<0.05, **p<0.01, *** p<0.0001.

Figure 6: Pluripotent markers in ΔTPR1 embryonic stem cells.

A. Immunofluorescence staining for STI1 (green), Sox2 (magenta) and Oct4 (red). Scale bar= 25µm. **B.** Sox2, STI1, Oct4 fluorescence intensity per colony in arbitrary units (a.u.). (N=5) **C.** Representative immunoblots from WT and ΔTPR1 embryonic stem cell populations lysates for Hsp90, STI1, Oct4 and Nanog with Actin as loading control**. D.** Densitometric quantification of protein levels (N=3). **E.** RT-qPCR for pluripotency markers. Expression levels are shown as fold change relative to WT murine ES cells. GAPDH was used for normalization. Error bars indicate

S.E.M from three biological replicates. **F.** Representative images for alkaline phosphatase staining of WT and ΔTPR1 cells (representative images at 40X magnification). **G.** Quantification of colonies in two sets of cultures of each genotype. AP+ (undifferentiated cells), AP- (differentiated cells) (N=3). Scale bar= 50 µm **H.** Immunofluorescence staining for SSEA1 (green) and Nanog (red). Scale bar= 30 µm. **I.** q-PCR of SSEA1 in ES cells, with GAPDH as reference gene (N=4). **J**. Histograms display SSEA1 flow cytometry profile in ΔTPR1 and WT cell populations (N=3).

Figure 7: Proliferation and cellular stress in ΔTPR1 embryonic stem cells.

A. Representative images of immunofluorescence staining for Ki67 (green) and Sox2 (red). Scale bars= 50 µm. **B.** Quantification of Ki67 positive cells. Error bars indicate the S.E.M of three independent assays. **C**. Growth rate of WT and ΔTPR1 (homozygous) embryonic stem cells. Graphs show the mean and S.E.M. of three independent experiments. **D**. Representative images of immunofluorescence staining for γ-H2AX (green) and DAPI (blue**).** Scale bars= 50 µm. **E.** Quantification of γ-H2AX positive nuclei. (N=3) **F**. Distribution of STI1 in ES cells differentiated. STI1 (green), Sox2 (red) and DAPI (blue). STI1 detection in the leading edge of migrating cells (arrows, WT left panel) and associated to cytoskeleton (arrowhead, WT left panel). Nuclear STI1 (arrowheads, ΔTPR1 left panel). Scale bars= 50 µm (N=3) **G**. Representative immunoblot for STI1 in un-and differentiated embryonic stem cells. **H.** Quantification of STI1 protein levels (N=3). *$p<0.05$, **$p<0.01$, *** $p<0.0001$.

Figure 8. Neurodegeneration in ΔTPR1 mice.

A. Representative images of silver staining in the dentate gyrus (at 20X magnification). Raw image and a thresholded image are shown to visualize silver particles. **B.** Quantitative analysis of silver particles in dentate gyrus (N=4/genotype). **C.** Silver staining in the CA1 region. **D.** Quantification of silver staining in the CA1 region. **E.** Silver staining in CA3 subfields, CAa, CA3b and CA3c. Arrows indicate noticeable thinning of CA3 neuronal layer in ΔTPR1 mice compared to littermate controls. **F-I.** Quantitative analysis of silver particles in hippocampal CA3 region. All data are Mean ± S.E.M. *$p<0.05$ Student's t-test. Scale bars 50 µm.

Figure 9. Neuronal loss in CA3 region and spatial memory deficits in ΔTPR1 mice.

A. Representative micrographs of NeuN staining in CA3 region of 3-5 month old male mice (at 10X magnification). **B-E.** Average NeuN positive neurons in all CA3 subfields per section. (N=4-5 animals/genotype). **F.** NeuN staining in the CA3 region of 14-16 month old mice (at 10X magnification). **G-J.** Average NeuN positive neurons per section relative to WT. Data analyzed using Student's t-test (N=4-5/genotype). **K-N.** Spatial Morris Water Maze test in 9 month old mice. Measures of learning during the acquisition phase of the task. **O.** Probe trial performance. Data analyzed using Two-Way ANOVA Repeat Measures. (n=9-10/genotype). All data are Mean ± S.E.M. *$p<0.05$, **$p<0.01$, *** $p<0.0001$. Scale bars represent 50 µm for 20X images and 150 µm for 10X images.

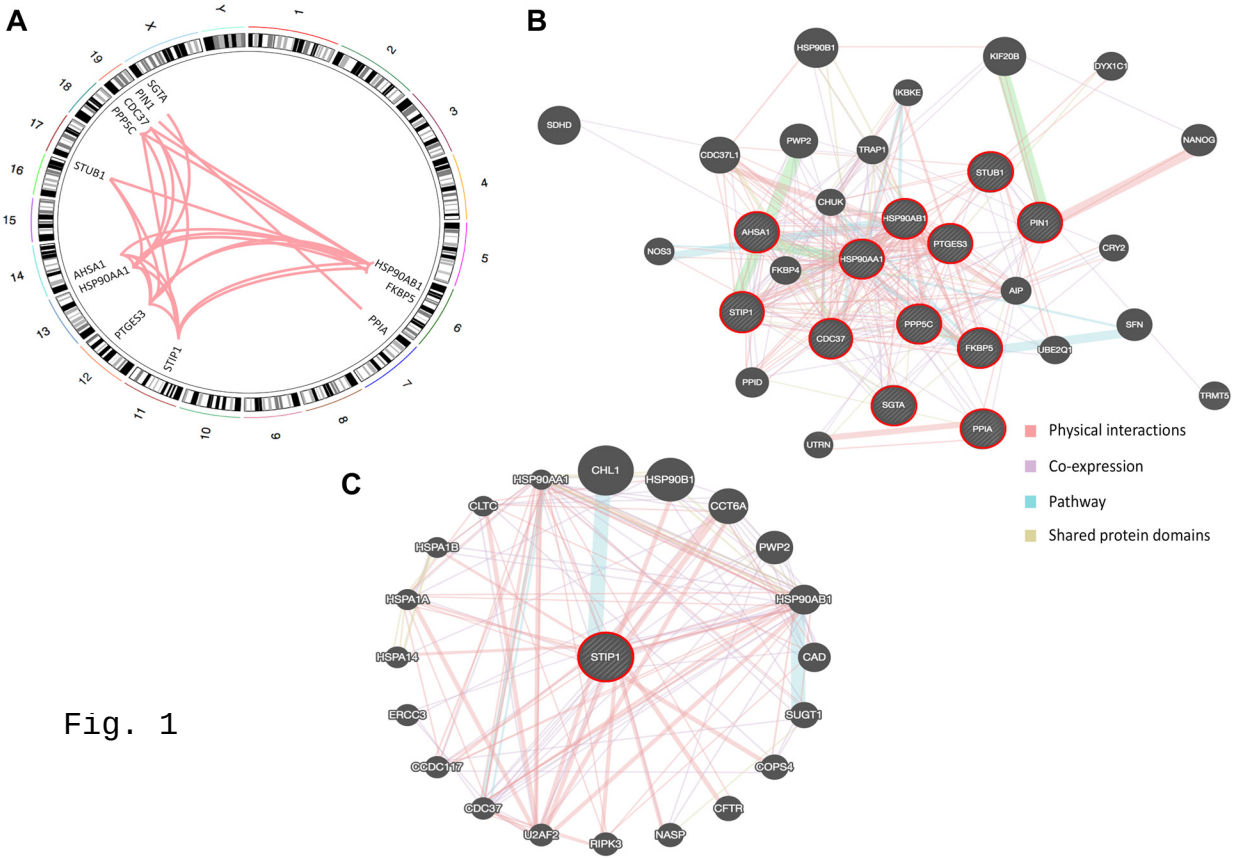
A
B
C
SGTA
PIN1
CDC37
PPP5C
STUB1
AHSA1
HSP90AA1
PTGES3
STIP1
HSP90AB1
FKBP5
PPIA
HSP90B1
KIF20B
DYX1C1
IKBKE
SDHD
PWP2
TRAP1
CDC37L1
NANOG
CHUK
NOS3
FKBP4
CRY2
AIP
SFN
UBE2Q1
PPID
TRMT5
UTRN
Physical interactions
Co-expression
Pathway
Shared protein domains
CHL1
CLTC
CCT6A
HSPA1B
HSPA1A
HSPA14
ERCC3
CCDC117
CDC37
U2AF2
RIPK3
NASP
CFTR
COPS4
SUGT1
CAD

Fig. 1

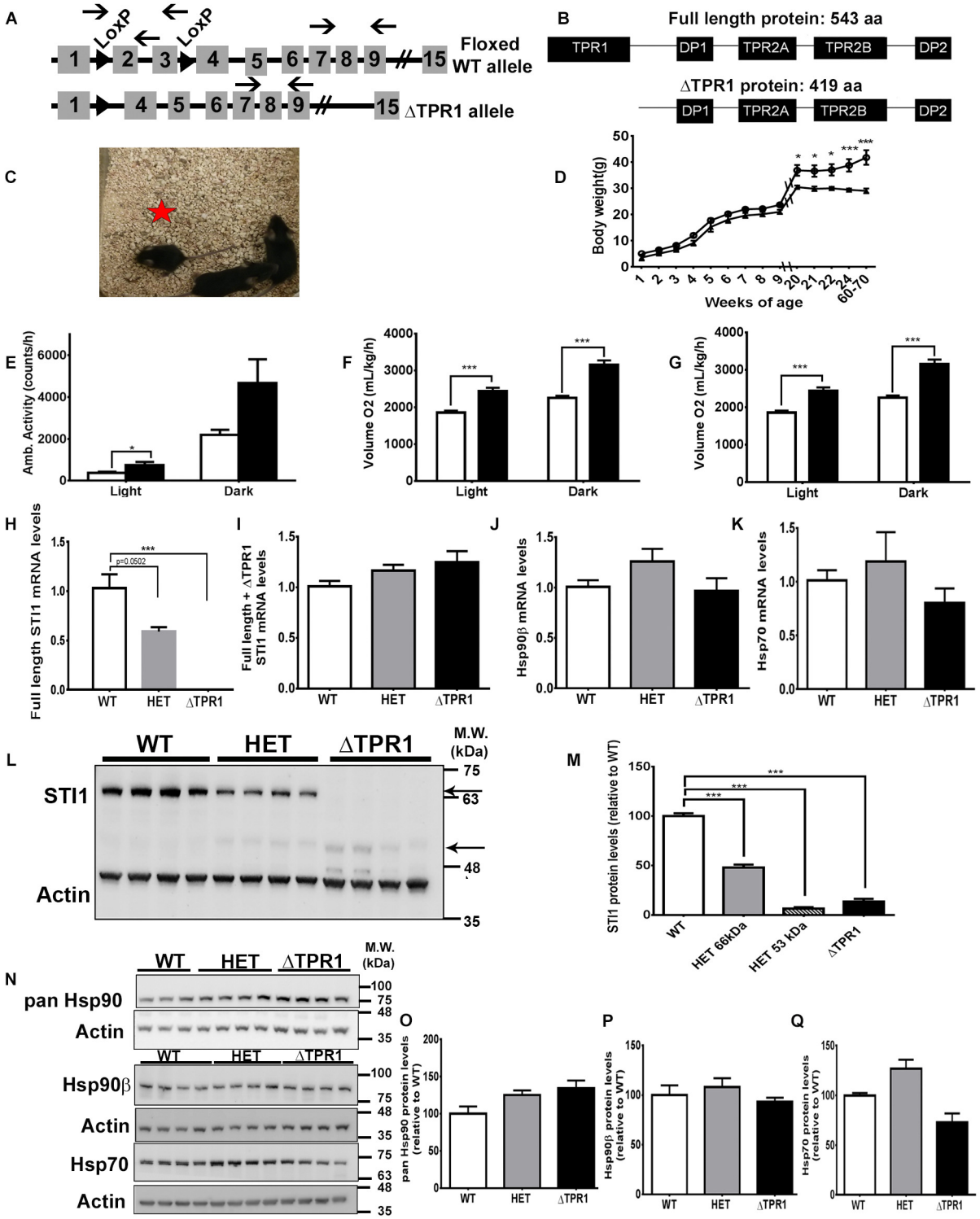
A
LoxP
LoxP
1 2 3 4 5 6 7 8 9 15
Floxed WT allele
1 4 5 6 7 8 9 15
ΔTPR1 allele
B
Full length protein: 543 aa
TPR1
DP1
TPR2A
TPR2B
DP2
ΔTPR1 protein: 419 aa
DP1
TPR2A
TPR2B
DP2
C
D
Body weight(g)
Weeks of age
E
Amb. Activity (counts/h)
Light
Dark
F
Volume O2 (mL/kg/h)
Light
Dark
G
Volume O2 (mL/kg/h)
Light
Dark
H
Full length STI1 mRNA levels
p=0.0502
WT
HET
ΔTPR1
I
Full length + ΔTPR1 STI1 mRNA levels
WT
HET
ΔTPR1
J
Hsp90β mRNA levels
WT
HET
ΔTPR1
K
Hsp70 mRNA levels
WT
HET
ΔTPR1
L
WT
HET
ΔTPR1
M.W. (kDa)
STI1
Actin
75
63
48
35
M
STI1 protein levels (relative to WT)
WT
HET 66kDa
HET 53 kDa
ΔTPR1
N
WT
HET
ΔTPR1
M.W. (kDa)
pan Hsp90
Actin
Hsp90β
Actin
Hsp70
Actin
O
pan Hsp90 protein levels (relative to WT)
WT
HET
ΔTPR1
P
Hsp90β protein levels (relative to WT)
WT
HET
ΔTPR1
Q
Hsp70 protein levels (relative to WT)
WT
HET
ΔTPR1

Fig. 2

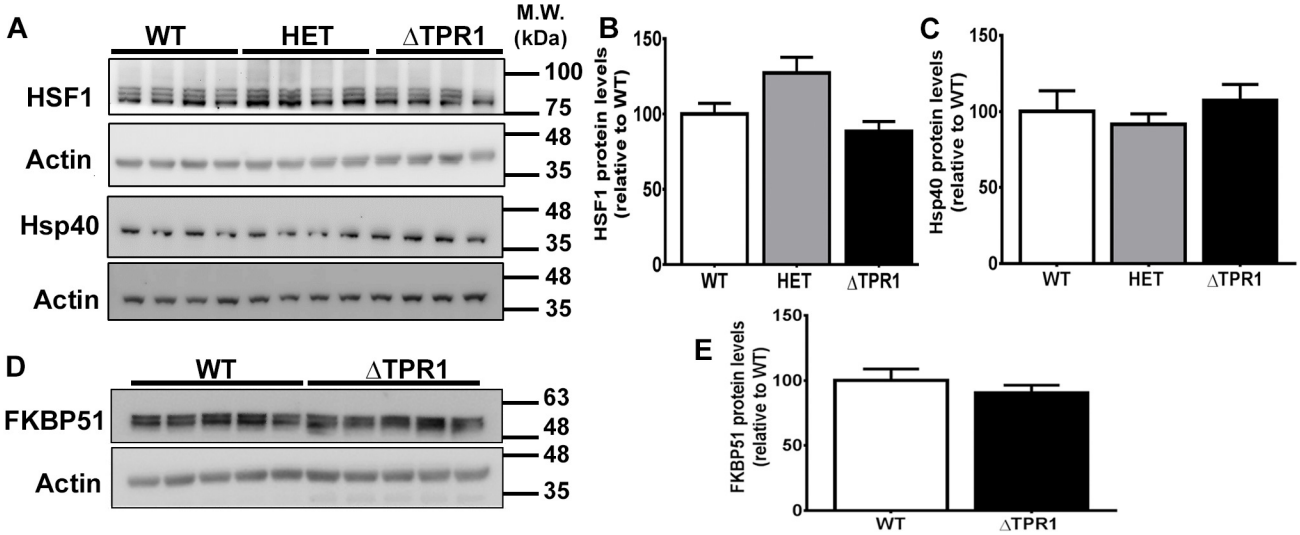
A
WT
HET
ΔTPR1
M.W. (kDa)
HSF1
Actin
Hsp40
Actin
100
75
48
35
48
35
48
35
B
HSF1 protein levels (relative to WT)
150
100
50
0
WT
HET
ΔTPR1
C
Hsp40 protein levels (relative to WT)
150
100
50
0
WT
HET
ΔTPR1
D
WT
ΔTPR1
FKBP51
Actin
63
48
48
35
E
FKBP51 protein levels (relative to WT)
150
100
50
0
WT
ΔTPR1

Fig. 3

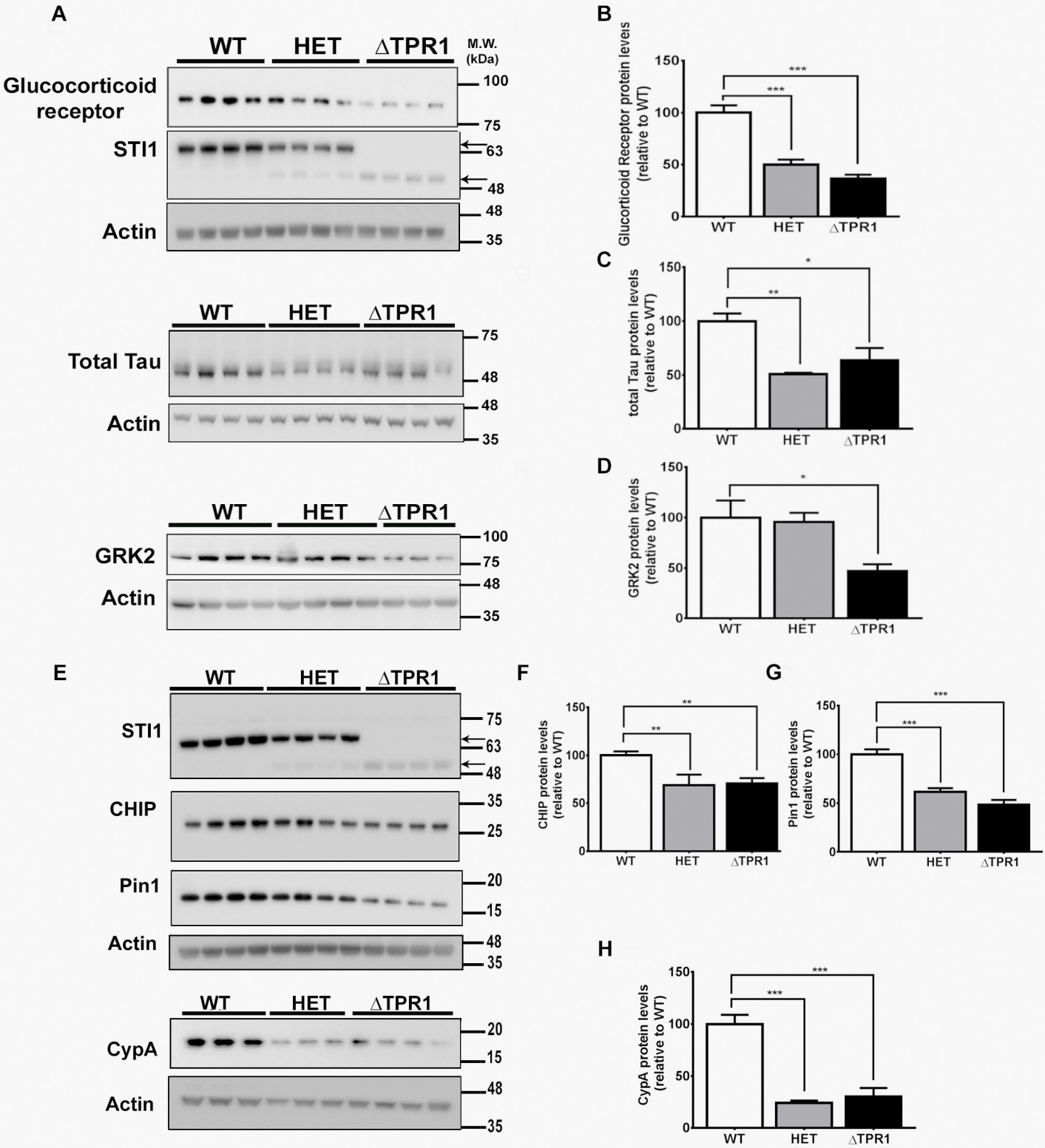
A
WT
HET
ΔTPR1
M.W. (kDa)
Glucocorticoid receptor
STI1
Actin
100
75
63
48
48
35
Total Tau
Actin
75
48
48
35
GRK2
Actin
100
75
48
35
B
Glucocorticoid Receptor protein levels (relative to WT)
150
100
50
0
***
***
WT
HET
ΔTPR1
C
total Tau protein levels (relative to WT)
*
**
D
GRK2 protein levels (relative to WT)
*
E
STI1
CHIP
Pin1
Actin
CypA
Actin
63
25
20
15
F
CHIP protein levels (relative to WT)
**
**
G
Pin1 protein levels (relative to WT)
***
***
H
CypA protein levels (relative to WT)
***
***

Fig. 4

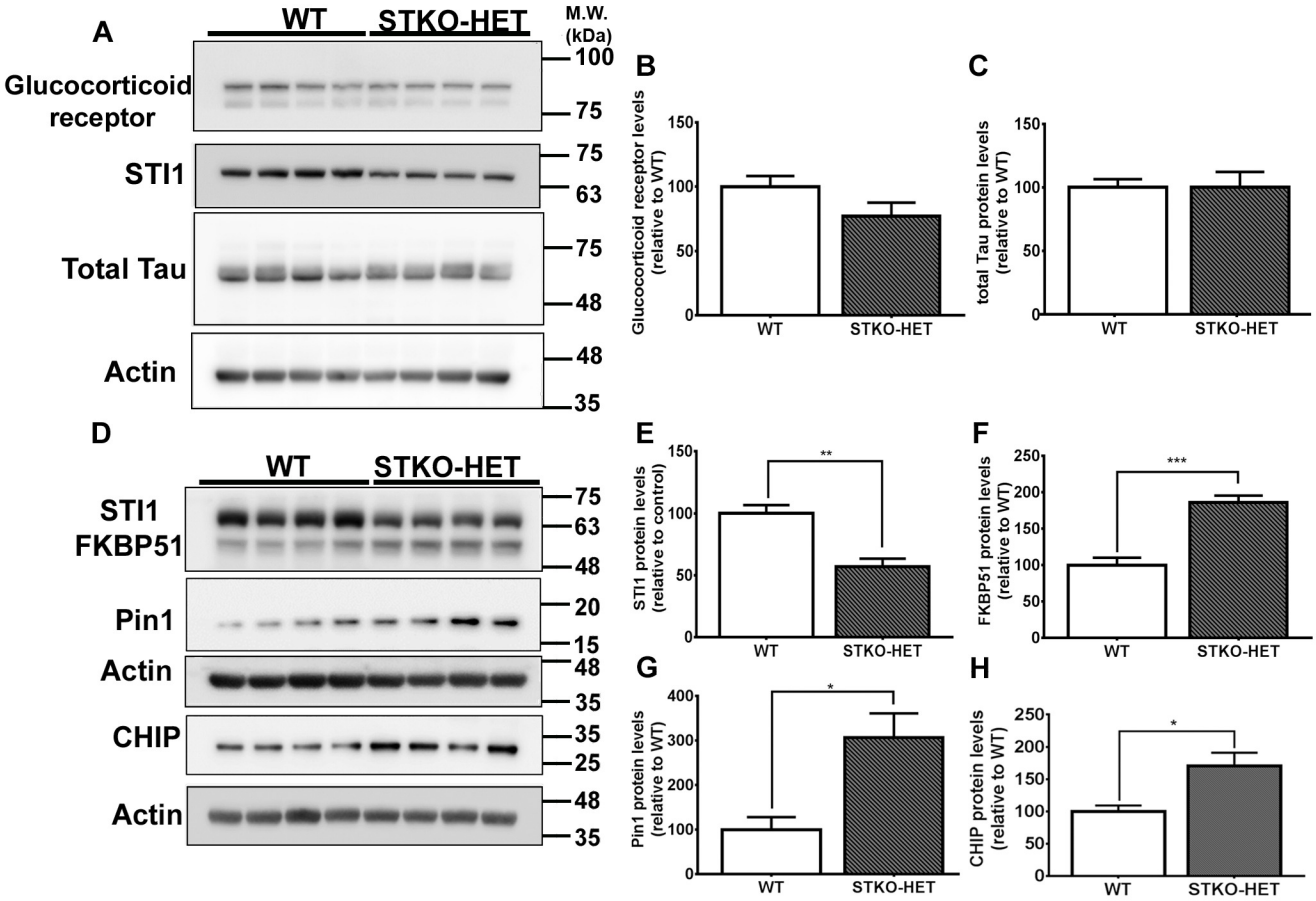
A
WT
STKO-HET
M.W. (kDa)
Glucocorticoid receptor
100
75
STI1
75
63
Total Tau
75
48
Actin
48
35
B
Glucocorticoid receptor levels (relative to WT)
150
100
50
0
WT
STKO-HET
C
total Tau protein levels (relative to WT)
150
100
50
0
WT
STKO-HET
D
WT
STKO-HET
STI1
FKBP51
75
63
48
Pin1
20
15
Actin
48
35
CHIP
35
25
Actin
48
35
E
STI1 protein levels (relative to control)
150
100
50
0
**
WT
STKO-HET
F
FKBP51 protein levels (relative to WT)
250
200
150
100
50
0
***
WT
STKO-HET
G
Pin1 protein levels (relative to WT)
400
300
200
100
0
*
WT
STKO-HET
H
CHIP protein levels (relative to WT)
250
200
150
100
50
0
*
WT
STKO-HET

Fig. 5

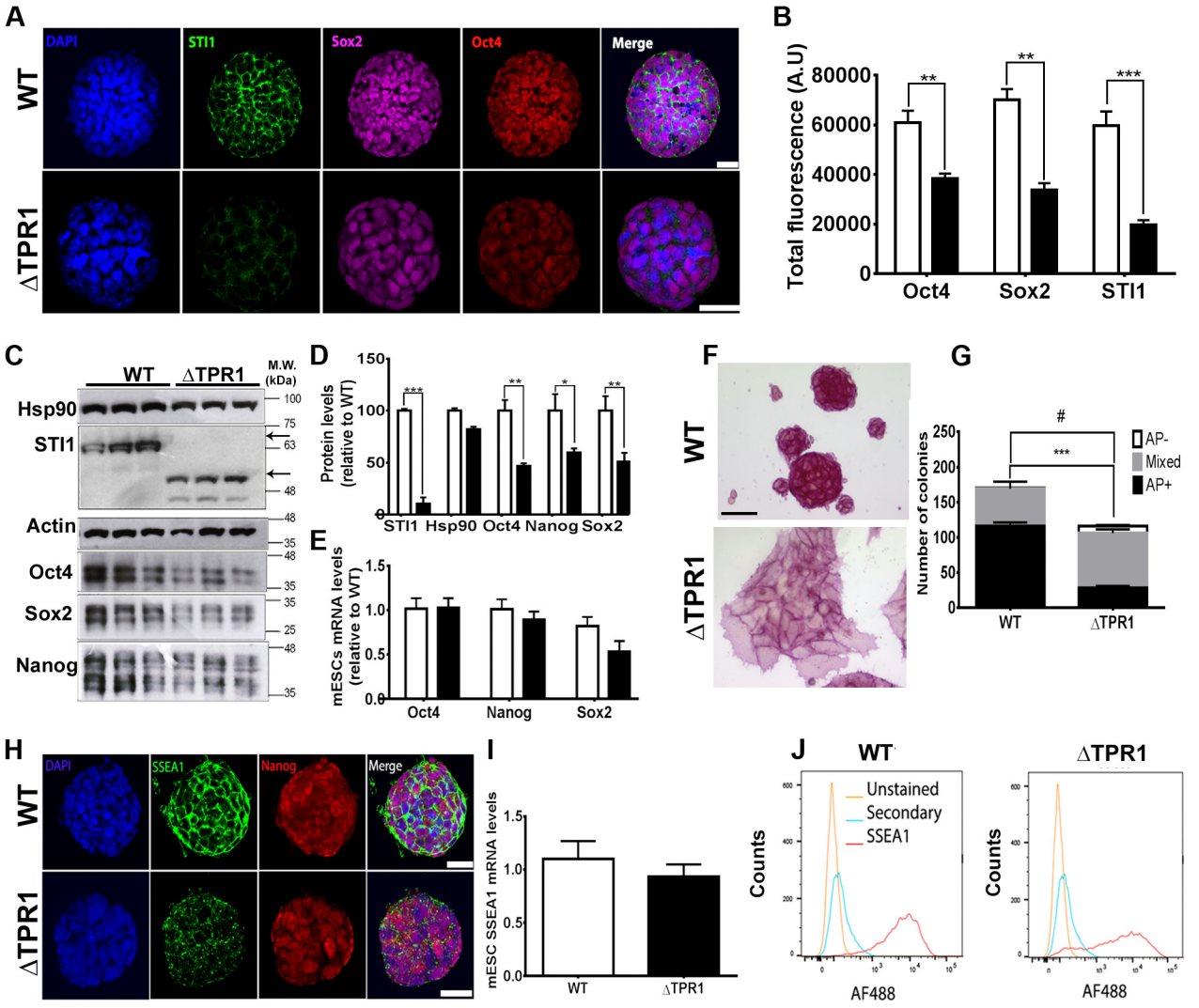
A
DAPI
STI1
Sox2
Oct4
Merge
WT
ΔTPR1
B
Total fluorescence (A.U)
80000
60000
40000
20000
0
Oct4
Sox2
STI1
C
WT
ΔTPR1
M.W. (kDa)
Hsp90
STI1
Actin
Oct4
Sox2
Nanog
D
Protein levels (relative to WT)
STI1 Hsp90 Oct4 Nanog Sox2
E
mESCs mRNA levels (relative to WT)
Oct4
Nanog
Sox2
F
WT
ΔTPR1
G
Number of colonies
AP-
Mixed
AP+
WT
ΔTPR1
H
DAPI
SSEA1
Nanog
Merge
WT
ΔTPR1
I
mESC SSEA1 mRNA levels
WT
ΔTPR1
J
WT
ΔTPR1
Unstained
Secondary
SSEA1
Counts
AF488

Fig. 6

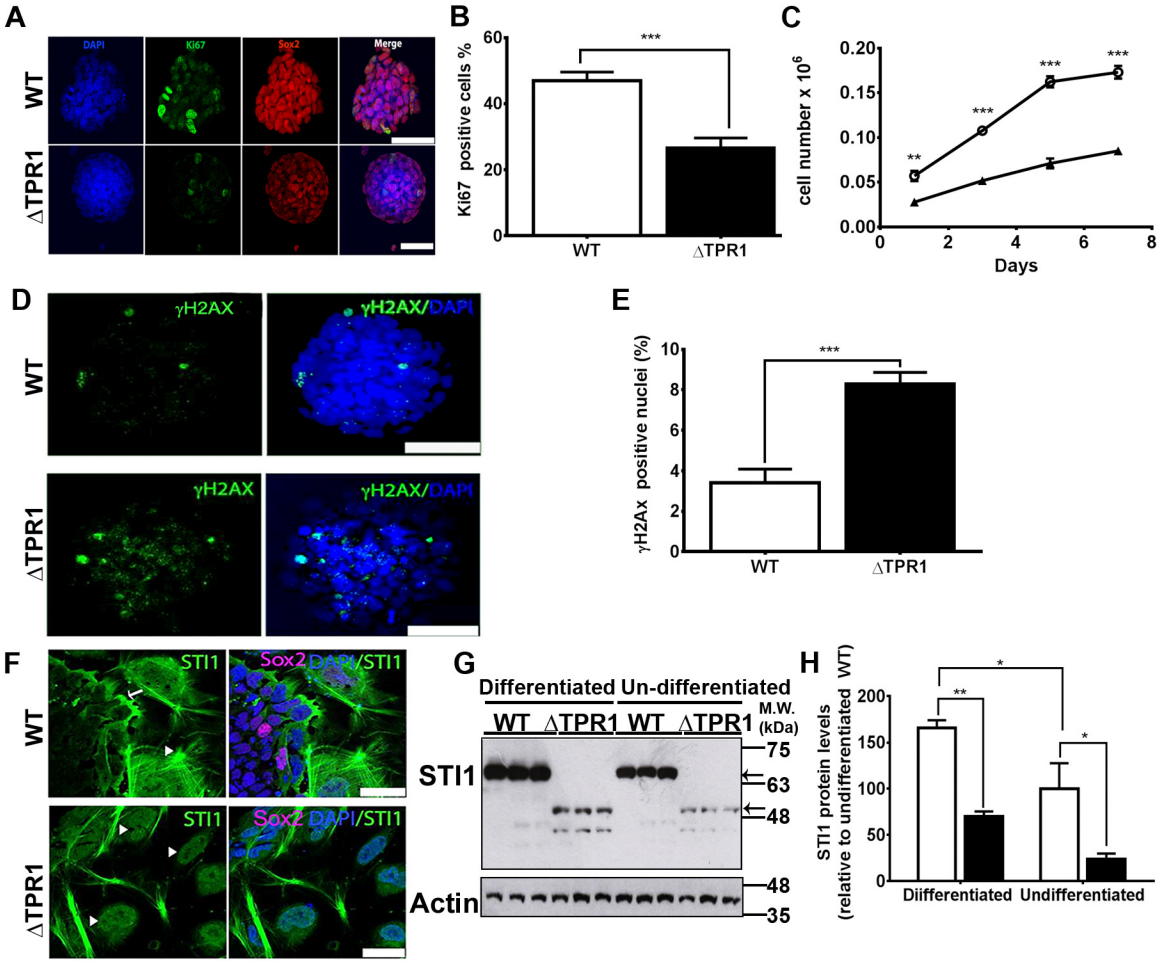
A
DAPI
Ki67
Sox2
Merge
WT
ΔTPR1
B
Ki67 positive cells %
60
40
20
0
***
WT
ΔTPR1
C
cell number x 10^6
0.20
0.15
0.10
0.05
0.00
**
***
***
***
0
2
4
6
8
Days
D
γH2AX
γH2AX/DAPI
WT
ΔTPR1
E
γH2Ax positive nuclei (%)
10
8
6
4
2
0
***
WT
ΔTPR1
F
STI1
Sox2 DAPI/STI1
WT
ΔTPR1
G
Differentiated
Un-differentiated
WT
ΔTPR1
WT
ΔTPR1
M.W. (kDa)
STI1
75
63
48
Actin
48
35
H
STI1 protein levels (relative to undifferentiated WT)
200
150
100
50
0
*
**
*
Differentiated
Undifferentiated

Fig. 7

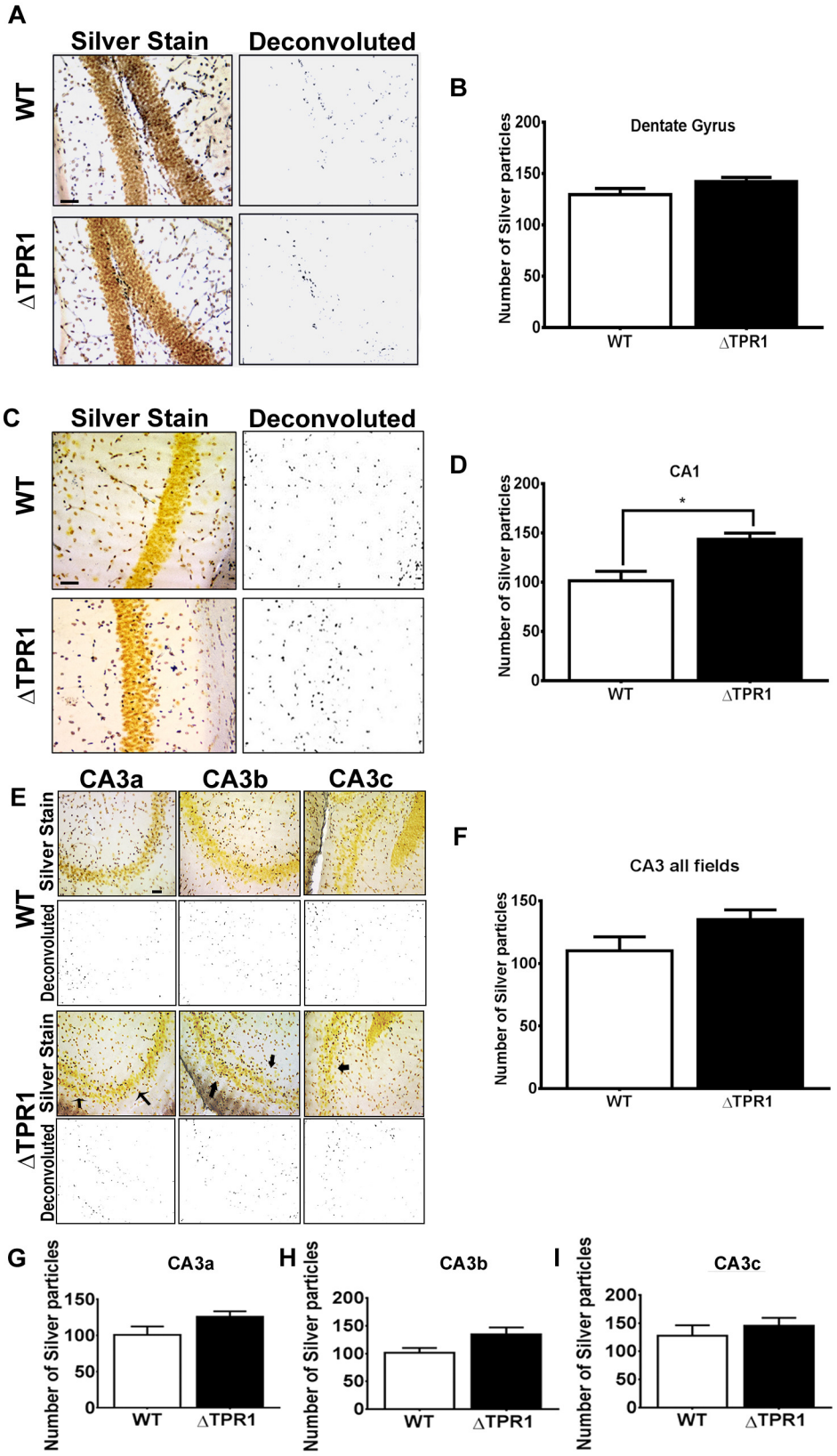
A
Silver Stain
Deconvoluted
WT
ΔTPR1
B
Dentate Gyrus
Number of Silver particles
200
150
100
50
0
WT
ΔTPR1
C
Silver Stain
Deconvoluted
WT
ΔTPR1
D
CA1
*
Number of Silver particles
200
150
100
50
0
WT
ΔTPR1
E
CA3a
CA3b
CA3c
Silver Stain
Deconvoluted
WT
ΔTPR1
F
CA3 all fields
Number of Silver particles
150
100
50
0
WT
ΔTPR1
G
CA3a
H
CA3b
I
CA3c
Number of Silver particles
WT
ΔTPR1

Fig. 8

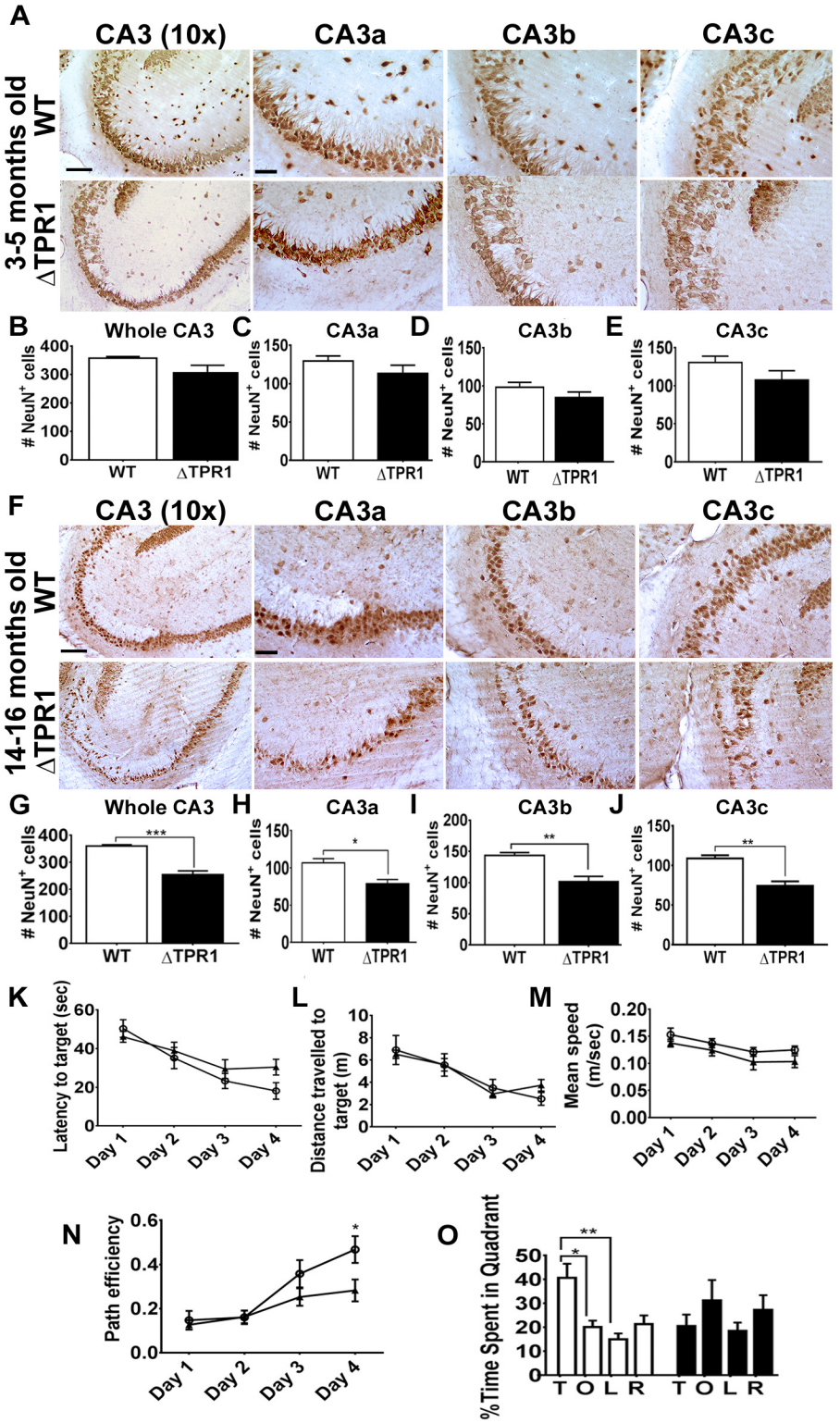
A
CA3 (10x)
CA3a
CA3b
CA3c
3-5 months old
WT
ΔTPR1
B
Whole CA3
C
CA3a
D
CA3b
E
CA3c
NeuN+ cells
WT
ΔTPR1
F
14-16 months old
G
H
I
J
***
*
**
K
Latency to target (sec)
L
Distance travelled to target (m)
M
Mean speed (m/sec)
Day 1
Day 2
Day 3
Day 4
N
Path efficiency
O
% Time Spent in Quadrant
T O L R

Fig. 9

References

1. Bradley E, Bieberich E, Mivechi NF, Tangpisuthipongsa D, Wang G (2012) Regulation of embryonic stem cell pluripotency by heat shock protein 90. Stem Cells 30: 1624-1633.
2. Beraldo FH, Soares IN, Goncalves DF, Fan J, Thomas AA, et al. (2013) Stress-inducible phosphoprotein 1 has unique cochaperone activity during development and regulates cellular response to ischemia via the prion protein. FASEB J 27: 3594-3607.
3. Brehme M, Voisine C, Rolland T, Wachi S, Soper JH, et al. (2014) A chaperome subnetwork safeguards proteostasis in aging and neurodegenerative disease. Cell Rep 9: 1135-1150.
4. Pratt WB, Gestwicki JE, Osawa Y, Lieberman AP (2015) Targeting Hsp90/Hsp70-based protein quality control for treatment of adult onset neurodegenerative diseases. Annu Rev Pharmacol Toxicol 55: 353-371.
5. Carman A, Kishinevsky S, Koren J, 3rd, Luo W, Chiosis G (2014) Regulatory chaperone complexes in neurodegenerative diseases: a perspective on therapeutic intervention. Curr Alzheimer Res 11: 59-68.
6. Fontaine SN, Zheng D, Sabbagh JJ, Martin MD, Chaput D, et al. (2016) DnaJ/Hsc70 chaperone complexes control the extracellular release of neurodegenerative-associated proteins. EMBO J 35: 1537-1549.
7. Hashimoto-Torii K, Torii M, Fujimoto M, Nakai A, El Fatimy R, et al. (2014) Roles of heat shock factor 1 in neuronal response to fetal environmental risks and its relevance to brain disorders. Neuron 82: 560-572.
8. Karam JA, Parikh RY, Nayak D, Rosenkranz D, Gangaraju VK (2017) Co-chaperone Hsp70/Hsp90-organizing protein (Hop) is required for transposon silencing and Piwi-interacting RNA (piRNA) biogenesis. J Biol Chem 292: 6039-6046.
9. Gangaraju VK, Yin H, Weiner MM, Wang J, Huang XA, et al. (2011) Drosophila Piwi functions in Hsp90-mediated suppression of phenotypic variation. Nat Genet 43: 153-158.
10. Johnson BD, Schumacher RJ, Ross ED, Toft DO (1998) Hop modulates Hsp70/Hsp90 interactions in protein folding. J Biol Chem 273: 3679-3686.
11. Schmid AB, Lagleder S, Grawert MA, Rohl A, Hagn F, et al. (2012) The architecture of functional modules in the Hsp90 co-chaperone Sti1/Hop. EMBO J.
12. Lee CT, Graf C, Mayer FJ, Richter SM, Mayer MP (2012) Dynamics of the regulation of Hsp90 by the co-chaperone Sti1. EMBO J 31: 1518-1528.
13. Rohl A, Wengler D, Madl T, Lagleder S, Tippel F, et al. (2015) Hsp90 regulates the dynamics of its cochaperone Sti1 and the transfer of Hsp70 between modules. Nat Commun 6: 6655.
14. Rohl A, Tippel F, Bender E, Schmid AB, Richter K, et al. (2015) Hop/Sti1 phosphorylation inhibits its co-chaperone function. EMBO Rep 16: 240-249.
15. Song HO, Lee W, An K, Lee HS, Cho JH, et al. (2009) C. elegans STI-1, the homolog of Sti1/Hop, is involved in aging and stress response. J Mol Biol 390: 604-617.
16. Nicolet CM, Craig EA (1989) Isolation and characterization of STI1, a stress-inducible gene from Saccharomyces cerevisiae. Mol Cell Biol 9: 3638-3646.
17. Piper PW, Millson SH, Mollapour M, Panaretou B, Siligardi G, et al. (2003) Sensitivity to Hsp90-targeting drugs can arise with mutation to the Hsp90 chaperone, cochaperones and plasma membrane ATP binding cassette transporters of yeast. Eur J Biochem 270: 4689-4695.
18. Chang HC, Nathan DF, Lindquist S (1997) In vivo analysis of the Hsp90 cochaperone Sti1 (p60). Mol Cell Biol 17: 318-325.

1007 19. Flom G, Behal RH, Rosen L, Cole DG, Johnson JL (2007) Definition of the minimal fragments of Sti1
1008 required for dimerization, interaction with Hsp70 and Hsp90 and in vivo functions. Biochem J
1009 404: 159-167.
1010 20. Flom G, Weekes J, Williams JJ, Johnson JL (2006) Effect of mutation of the tetratricopeptide repeat
1011 and asparatate-proline 2 domains of Sti1 on Hsp90 signaling and interaction in Saccharomyces
1012 cerevisiae. Genetics 172: 41-51.
1013 21. Song Y, Masison DC (2005) Independent regulation of Hsp70 and Hsp90 chaperones by
1014 Hsp70/Hsp90-organizing protein Sti1 (Hop1). J Biol Chem 280: 34178-34185.
1015 22. Lek M, Karczewski KJ, Minikel EV, Samocha KE, Banks E, et al. (2016) Analysis of protein-coding
1016 genetic variation in 60,706 humans. Nature 536: 285-291.
1017 23. Grad I, Cederroth CR, Walicki J, Grey C, Barluenga S, et al. (2010) The molecular chaperone
1018 Hsp90alpha is required for meiotic progression of spermatocytes beyond pachytene in the
1019 mouse. PLoS ONE 5: e15770.
1020 24. Voss AK, Thomas T, Gruss P (2000) Mice lacking HSP90beta fail to develop a placental labyrinth.
1021 Development 127: 1-11.
1022 25. Felts SJ, Toft DO (2003) p23, a simple protein with complex activities. Cell Stress Chaperones 8: 108-
1023 113.
1024 26. Grad I, McKee TA, Ludwig SM, Hoyle GW, Ruiz P, et al. (2006) The Hsp90 cochaperone p23 is
1025 essential for perinatal survival. MolCell Biol 26: 8976-8983.
1026 27. Li J, Soroka J, Buchner J (2012) The Hsp90 chaperone machinery: Conformational dynamics and
1027 regulation by co-chaperones. BiochimBiophysActa 1823: 624-635.
1028 28. Retzlaff M, Hagn F, Mitschke L, Hessling M, Gugel F, et al. (2010) Asymmetric activation of the hsp90
1029 dimer by its cochaperone aha1. MolCell 37: 344-354.
1030 29. Yong W, Yang Z, Periyasamy S, Chen H, Yucel S, et al. (2007) Essential role for Co-chaperone Fkbp52
1031 but not Fkbp51 in androgen receptor-mediated signaling and physiology. J Biol Chem 282: 5026-
1032 5036.
1033 30. MacLean M, Picard D (2003) Cdc37 goes beyond Hsp90 and kinases. Cell StressChaperones 8: 114-
1034 119.
1035 31. Beers M, Kemphues K (2006) Depletion of the co-chaperone CDC-37 reveals two modes of PAR-6
1036 cortical association in C. elegans embryos. Development 133: 3745-3754.
1037 32. Philp LK, Day TK, Butler MS, Laven-Law G, Jindal S, et al. (2016) Small Glutamine-Rich
1038 Tetratricopeptide Repeat-Containing Protein Alpha (SGTA) Ablation Limits Offspring Viability and
1039 Growth in Mice. Sci Rep 6: 28950.
1040 33. Yong W, Bao S, Chen H, Li D, Sanchez ER, et al. (2007) Mice lacking protein phosphatase 5 are
1041 defective in ataxia telangiectasia mutated (ATM)-mediated cell cycle arrest. J Biol Chem 282:
1042 14690-14694.
1043 34. Beraldo FH, Thomas A, Kolisnyk B, Hirata PH, De Jaeger X, et al. (2015) Hyperactivity and attention
1044 deficits in mice with decreased levels of stress-inducible phosphoprotein 1 (STIP1). Dis Model
1045 Mech 8: 1457-1466.
1046 35. Sawarkar R, Sievers C, Paro R (2012) Hsp90 globally targets paused RNA polymerase to regulate gene
1047 expression in response to environmental stimuli. Cell 149: 807-818.
1048 36. Dai Q, Zhang C, Wu Y, McDonough H, Whaley RA, et al. (2003) CHIP activates HSF1 and confers
1049 protection against apoptosis and cellular stress. Embo j 22: 5446-5458.
1050 37. Zou J, Guo Y, Guettouche T, Smith DF, Voellmy R (1998) Repression of heat shock transcription factor
1051 HSF1 activation by HSP90 (HSP90 complex) that forms a stress-sensitive complex with HSF1. Cell
1052 94: 471-480.

1053 38. Wang B, Liu Y, Huang L, Chen J, Li JJ, et al. (2016) A CNS-permeable Hsp90 inhibitor rescues synaptic
1054 dysfunction and memory loss in APP-overexpressing Alzheimer's mouse model via an HSF1-
1055 mediated mechanism. Mol Psychiatry.
1056 39. Chen Y, Wang B, Liu D, Li JJ, Xue Y, et al. (2014) Hsp90 chaperone inhibitor 17-AAG attenuates Abeta-
1057 induced synaptic toxicity and memory impairment. J Neurosci 34: 2464-2470.
1058 40. Verma P, Pfister JA, Mallick S, D'Mello SR (2014) HSF1 protects neurons through a novel
1059 trimerization- and HSP-independent mechanism. J Neurosci 34: 1599-1612.
1060 41. Ding Y, Adachi H, Katsuno M, Sahashi K, Kondo N, et al. (2016) BIIB021, a synthetic Hsp90 inhibitor,
1061 induces mutant ataxin-1 degradation through the activation of heat shock factor 1.
1062 Neuroscience 327: 20-31.
1063 42. Morgner N, Schmidt C, Beilsten-Edmands V, Ebong IO, Patel NA, et al. (2015) Hsp70 forms
1064 antiparallel dimers stabilized by post-translational modifications to position clients for transfer
1065 to Hsp90. Cell Rep 11: 759-769.
1066 43. Cyr DM, Lu X, Douglas MG (1992) Regulation of Hsp70 function by a eukaryotic DnaJ homolog. J Biol
1067 Chem 267: 20927-20931.
1068 44. Frydman J, Nimmesgern E, Ohtsuka K, Hartl FU (1994) Folding of nascent polypeptide chains in a high
1069 molecular mass assembly with molecular chaperones. Nature 370: 111-117.
1070 45. Tsai J, Douglas MG (1996) A conserved HPD sequence of the J-domain is necessary for YDJ1
1071 stimulation of Hsp70 ATPase activity at a site distinct from substrate binding. J Biol Chem 271:
1072 9347-9354.
1073 46. Dickey CA, Kamal A, Lundgren K, Klosak N, Bailey RM, et al. (2007) The high-affinity HSP90-CHIP
1074 complex recognizes and selectively degrades phosphorylated tau client proteins. J Clin Invest
1075 117: 648-658.
1076 47. Jinwal UK, Koren J, 3rd, Borysov SI, Schmid AB, Abisambra JF, et al. (2010) The Hsp90 cochaperone,
1077 FKBP51, increases Tau stability and polymerizes microtubules. J Neurosci 30: 591-599.
1078 48. Barent RL, Nair SC, Carr DC, Ruan Y, Rimerman RA, et al. (1998) Analysis of FKBP51/FKBP52 chimeras
1079 and mutants for Hsp90 binding and association with progesterone receptor complexes. Mol
1080 Endocrinol 12: 342-354.
1081 49. Nair SC, Rimerman RA, Toran EJ, Chen S, Prapapanich V, et al. (1997) Molecular cloning of human
1082 FKBP51 and comparisons of immunophilin interactions with Hsp90 and progesterone receptor.
1083 Mol Cell Biol 17: 594-603.
1084 50. Wang W, Liu Y, Zhao Z, Xie C, Xu Y, et al. (2016) Y-632 inhibits heat shock protein 90 (Hsp90) function
1085 by disrupting the interaction between Hsp90 and Hsp70/Hsp90 organizing protein, and exerts
1086 antitumor activity in vitro and in vivo. Cancer Sci 107: 782-790.
1087 51. Pimienta G, Herbert KM, Regan L (2011) A compound that inhibits the HOP-Hsp90 complex
1088 formation and has unique killing effects in breast cancer cell lines. MolPharm 8: 2252-2261.
1089 52. Muller P, Ruckova E, Halada P, Coates PJ, Hrstka R, et al. (2013) C-terminal phosphorylation of Hsp70
1090 and Hsp90 regulates alternate binding to co-chaperones CHIP and HOP to determine cellular
1091 protein folding/degradation balances. Oncogene 32: 3101-3110.
1092 53. Petrucelli L, Dickson D, Kehoe K, Taylor J, Snyder H, et al. (2004) CHIP and Hsp70 regulate tau
1093 ubiquitination, degradation and aggregation. Hum Mol Genet 13: 703-714.
1094 54. Fujimori F, Takahashi K, Uchida C, Uchida T (1999) Mice lacking Pin1 develop normally, but are
1095 defective in entering cell cycle from G(0) arrest. Biochem Biophys Res Commun 265: 658-663.
1096 55. Colgan J, Asmal M, Neagu M, Yu B, Schneidkraut J, et al. (2004) Cyclophilin A regulates TCR signal
1097 strength in CD4+ T cells via a proline-directed conformational switch in Itk. Immunity 21: 189-
1098 201.
1099 56. Lee HJ, Gutierrez-Garcia R, Vilchez D (2017) Embryonic stem cells: a novel paradigm to study
1100 proteostasis? FEBS J 284: 391-398.

1101 57. Fan GC (2012) Role of heat shock proteins in stem cell behavior. Prog Mol Biol Transl Sci 111: 305-
1102 322.
1103 58. Longshaw VM, Baxter M, Prewitz M, Blatch GL (2009) Knockdown of the co-chaperone Hop
1104 promotes extranuclear accumulation of Stat3 in mouse embryonic stem cells. Eur J Cell Biol 88:
1105 153-166.
1106 59. Soares IN, Caetano FA, Pinder J, Rodrigues BR, Beraldo FH, et al. (2013) Regulation of stress-inducible
1107 phosphoprotein 1 nuclear retention by protein inhibitor of activated STAT PIAS1. Mol Cell
1108 Proteomics 12: 3253-3270.
1109 60. Lu T, Pan Y, Kao SY, Li C, Kohane I, et al. (2004) Gene regulation and DNA damage in the ageing
1110 human brain. Nature 429: 883-891.
1111 61. Lee CK, Weindruch R, Prolla TA (2000) Gene-expression profile of the ageing brain in mice. Nat Genet
1112 25: 294-297.
1113 62. Yoo BC, Kim SH, Cairns N, Fountoulakis M, Lubec G (2001) Deranged expression of molecular
1114 chaperones in brains of patients with Alzheimer's disease. Biochem Biophys Res Commun 280:
1115 249-258.
1116 63. Padurariu M, Ciobica A, Mavroudis I, Fotiou D, Baloyannis S (2012) Hippocampal neuronal loss in the
1117 CA1 and CA3 areas of Alzheimer's disease patients. Psychiatr Danub 24: 152-158.
1118 64. Kuhn HG, Dickinson-Anson H, Gage FH (1996) Neurogenesis in the dentate gyrus of the adult rat:
1119 age-related decrease of neuronal progenitor proliferation. J Neurosci 16: 2027-2033.
1120 65. Li JS, Chao YS (2008) Electrolytic lesions of dorsal CA3 impair episodic-like memory in rats. Neurobiol
1121 Learn Mem 89: 192-198.
1122 66. Gemmell E, Bosomworth H, Allan L, Hall R, Khundakar A, et al. (2012) Hippocampal neuronal atrophy
1123 and cognitive function in delayed poststroke and aging-related dementias. Stroke 43: 808-814.
1124 67. Kolisnyk B, Al-Onaizi M, Soreq L, Barbash S, Bekenstein U, et al. (2016) Cholinergic Surveillance over
1125 Hippocampal RNA Metabolism and Alzheimer's-Like Pathology. Cereb Cortex.
1126 68. Zhou H, Huang C, Chen H, Wang D, Landel CP, et al. (2010) Transgenic rat model of
1127 neurodegeneration caused by mutation in the TDP gene. PLoS Genet 6: e1000887.
1128 69. Chen Z, Shin D, Chen S, Mikhail K, Hadass O, et al. (2014) Histological quantitation of brain injury
1129 using whole slide imaging: a pilot validation study in mice. PLoS One 9: e92133.
1130 70. Chen L, Ding Y, Cagniard B, Van Laar AD, Mortimer A, et al. (2008) Unregulated cytosolic dopamine
1131 causes neurodegeneration associated with oxidative stress in mice. J Neurosci 28: 425-433.
1132 71. Farovik A, Dupont LM, Eichenbaum H (2010) Distinct roles for dorsal CA3 and CA1 in memory for
1133 sequential nonspatial events. Learn Mem 17: 12-17.
1134 72. Lee I, Jerman TS, Kesner RP (2005) Disruption of delayed memory for a sequence of spatial locations
1135 following CA1- or CA3-lesions of the dorsal hippocampus. Neurobiol Learn Mem 84: 138-147.
1136 73. Steffenach HA, Sloviter RS, Moser EI, Moser MB (2002) Impaired retention of spatial memory after
1137 transection of longitudinally oriented axons of hippocampal CA3 pyramidal cells. Proc Natl Acad
1138 Sci U S A 99: 3194-3198.
1139 74. Gaiser AM, Brandt F, Richter K (2009) The Non-canonical Hop Protein from Caenorhabditis elegans
1140 Exerts Essential Functions and Forms Binary Complexes with Either Hsc70 or Hsp90. JMolBiol.
1141 75. Schmid AB, Lagleder S, Grawert MA, Rohl A, Hagn F, et al. (2012) The architecture of functional
1142 modules in the Hsp90 co-chaperone Sti1/Hop. EMBO J 31: 1506-1517.
1143 76. van der Spuy J, Cheetham ME, Dirr HW, Blatch GL (2001) The cochaperone murine stress-inducible
1144 protein 1: overexpression, purification, and characterization. Protein Expr Purif 21: 462-469.
1145 77. Yi F, Doudevski I, Regan L (2010) HOP is a monomer: investigation of the oligomeric state of the co-
1146 chaperone HOP. Protein Sci 19: 19-25.

1147 78. Zininga T, Makumire S, Gitau GW, Njunge JM, Pooe OJ, et al. (2015) Plasmodium falciparum Hop
1148 (PfHop) Interacts with the Hsp70 Chaperone in a Nucleotide-Dependent Fashion and Exhibits
1149 Ligand Selectivity. PLoS One 10: e0135326.
1150 79. Sahasrabudhe P, Rohrberg J, Biebl MM, Rutz DA, Buchner J (2017) The Plasticity of the Hsp90 Co-
1151 chaperone System. Mol Cell 67: 947-961 e945.
1152 80. Noormohammadi A, Calculli G, Gutierrez-Garcia R, Khodakarami A, Koyuncu S, et al. (2017)
1153 Mechanisms of protein homeostasis (proteostasis) maintain stem cell identity in mammalian
1154 pluripotent stem cells. Cell Mol Life Sci.
1155 81. Kim YE, Hipp MS, Bracher A, Hayer-Hartl M, Hartl FU (2013) Molecular chaperone functions in
1156 protein folding and proteostasis. Annu Rev Biochem 82: 323-355.
1157 82. Vilchez D, Boyer L, Morantte I, Lutz M, Merkwirth C, et al. (2012) Increased proteasome activity in
1158 human embryonic stem cells is regulated by PSMD11. Nature 489: 304-308.
1159 83. Watanabe Y, Gould E, McEwen BS (1992) Stress induces atrophy of apical dendrites of hippocampal
1160 CA3 pyramidal neurons. Brain Res 588: 341-345.
1161 84. Kruman, II, Kumaravel TS, Lohani A, Pedersen WA, Cutler RG, et al. (2002) Folic acid deficiency and
1162 homocysteine impair DNA repair in hippocampal neurons and sensitize them to amyloid toxicity
1163 in experimental models of Alzheimer's disease. J Neurosci 22: 1752-1762.
1164 85. Gilbert PE, Brushfield AM (2009) The role of the CA3 hippocampal subregion in spatial memory: a
1165 process oriented behavioral assessment. Prog Neuropsychopharmacol Biol Psychiatry 33: 774-
1166 781.
1167 86. Lackie RE, Maciejewski A, Ostapchenko VG, Marques-Lopes J, Choy WY, et al. (2017) The
1168 Hsp70/Hsp90 Chaperone Machinery in Neurodegenerative Diseases. Front Neurosci 11: 254.
1169 87. Rodina A, Wang T, Yan P, Gomes ED, Dunphy MP, et al. (2016) The epichaperome is an integrated
1170 chaperome network that facilitates tumour survival. Nature 538: 397-401.
1171 88. Jhaveri K, Taldone T, Modi S, Chiosis G (2012) Advances in the clinical development of heat shock
1172 protein 90 (Hsp90) inhibitors in cancers. Biochim Biophys Acta 1823: 742-755.
1173 89. Fuhrmann-Stroissnigg H, Ling YY, Zhao J, McGowan SJ, Zhu Y, et al. (2017) Identification of HSP90
1174 inhibitors as a novel class of senolytics. Nat Commun 8: 422.
1175 90. Consortium GT (2013) The Genotype-Tissue Expression (GTEx) project. Nat Genet 45: 580-585.
1176 91. MacArthur J, Bowler E, Cerezo M, Gil L, Hall P, et al. (2017) The new NHGRI-EBI Catalog of published
1177 genome-wide association studies (GWAS Catalog). Nucleic Acids Res 45: D896-D901.
1178 92. Mick E, McGough J, Loo S, Doyle AE, Wozniak J, et al. (2011) Genome-wide association study of the
1179 child behavior checklist dysregulation profile. J Am Acad Child Adolesc Psychiatry 50: 807-817
1180 e808.
1181 93. Landrum MJ, Lee JM, Benson M, Brown G, Chao C, et al. (2016) ClinVar: public archive of
1182 interpretations of clinically relevant variants. Nucleic Acids Res 44: D862-868.
1183 94. Miller DT, Adam MP, Aradhya S, Biesecker LG, Brothman AR, et al. (2010) Consensus statement:
1184 chromosomal microarray is a first-tier clinical diagnostic test for individuals with developmental
1185 disabilities or congenital anomalies. Am J Hum Genet 86: 749-764.
1186 95. Stenson PD, Mort M, Ball EV, Evans K, Hayden M, et al. (2017) The Human Gene Mutation Database:
1187 towards a comprehensive repository of inherited mutation data for medical research, genetic
1188 diagnosis and next-generation sequencing studies. Hum Genet 136: 665-677.
1189 96. Firth HV, Richards SM, Bevan AP, Clayton S, Corpas M, et al. (2009) DECIPHER: Database of
1190 Chromosomal Imbalance and Phenotype in Humans Using Ensembl Resources. Am J Hum Genet
1191 84: 524-533.
1192 97. Kozak M (1986) Point mutations define a sequence flanking the AUG initiator codon that modulates
1193 translation by eukaryotic ribosomes. Cell 44: 283-292.

1194 98. Migliorini D, Lazzerini Denchi E, Danovi D, Jochemsen A, Capillo M, et al. (2002) Mdm4 (Mdmx)
1195 regulates p53-induced growth arrest and neuronal cell death during early embryonic mouse
1196 development. Mol Cell Biol 22: 5527-5538.
1197 99. Czechanski A, Byers C, Greenstein I, Schrode N, Donahue LR, et al. (2014) Derivation and
1198 characterization of mouse embryonic stem cells from permissive and nonpermissive strains. Nat
1199 Protoc 9: 559-574.
1200 100. Etoc F, Metzger J, Ruzo A, Kirst C, Yoney A, et al. (2016) A Balance between Secreted Inhibitors and
1201 Edge Sensing Controls Gastruloid Self-Organization. Dev Cell 39: 302-315.
1202 101. Afgan E, Baker D, van den Beek M, Blankenberg D, Bouvier D, et al. (2016) The Galaxy platform for
1203 accessible, reproducible and collaborative biomedical analyses: 2016 update. Nucleic Acids Res
1204 44: W3-W10.
1205 102. Kim D, Pertea G, Trapnell C, Pimentel H, Kelley R, et al. (2013) TopHat2: accurate alignment of
1206 transcriptomes in the presence of insertions, deletions and gene fusions. Genome Biol 14: R36.
1207 103. Anders S, Pyl PT, Huber W (2015) HTSeq--a Python framework to work with high-throughput
1208 sequencing data. Bioinformatics 31: 166-169.
1209 104. Love MI, Huber W, Anders S (2014) Moderated estimation of fold change and dispersion for RNA-
1210 seq data with DESeq2. Genome Biol 15: 550.
1211 105. Team RC (2017) R: A language and environment for statistical computing. R Foundation for
1212 Statistical Computing.
1213 106. Beraldo FH, Ostapchenko VG, Caetano FA, Guimaraes AL, Ferretti GD, et al. (2016) Regulation of
1214 Amyloid beta Oligomer Binding to Neurons and Neurotoxicity by the Prion Protein-mGluR5
1215 Complex. J Biol Chem 291: 21945-21955.
1216 107. Maciejewski A, Ostapchenko VG, Beraldo FH, Prado VF, Prado MA, et al. (2016) Domains of STIP1
1217 responsible for regulating the PrPC-dependent amyloid-beta oligomer toxicity. Biochem J.
1218 108. Guzman MS, De Jaeger X, Raulic S, Souza IA, Li AX, et al. (2011) Elimination of the vesicular
1219 acetylcholine transporter in the striatum reveals regulation of behaviour by cholinergic-
1220 glutamatergic co-transmission. PLoS Biol 9: e1001194.
1221 109. Kolisnyk B, Guzman MS, Raulic S, Fan J, Magalhaes AC, et al. (2013) ChAT-ChR2-EYFP mice have
1222 enhanced motor endurance but show deficits in attention and several additional cognitive
1223 domains. J Neurosci 33: 10427-10438.

1224

1225

1226

Supplementary materials

Supplementary Tables 1-3

Supplementary Figure 1. Metabolic Assessments of ΔTPR1 mice. Additional parameters were measured to investigate the leaner phenotype observed in ΔTPR1 mice such as **A.** Respiratory Exchange Ratio, **B.** Energy Expenditure, **C.** Food consumed, **D.** Water consumed, **E.** Sleep time. Data analyzed using Two-Way ANOVA Repeated Measures. n=7-8 mice/genotype with adult mice ranging in age from 8-12 months of age. *p<0.05.

Supplementary Figure 2. MEF mRNA expression and Hsp70 and Hsp90 cellular localization. A. Expression levels of full length STI1 mRNA using primers for exons 2 and 3 and **B.** Expression levels of full length + ΔTPR1 STI1 mRNA using primers for exons 8 and 9. (n=4 for qPCR experiments, data analyzed using One-way ANOVA). **C.** SPR analysis of affinity of STI1 antibody [Bethyl, (Beraldo et al, 2013)] for each domain of STI1. **p<0.001. **D-E.** Immunofluoresce analysis of the localization of Hsp90 (red); Hsp70 (red) and STI1 (green) in MEFs. Scale bar= 50 µm.

Supplementary Figure 3. Unaltered Transcriptome in ΔTPR1 mice. Transcriptional changes between RNA samples from the cortex of 5 STI1 WT and 5 STI1 ΔTPR1 mice were analyzed by long RNA-sequencing. Bioinformatic analysis showed minimal variance between the samples in both A) sample distance matrix and B) principal component analysis.

Supplementary Figure 4. mRNA levels of co-chaperones and Hsp90 client proteins. A. *Nr3c1* for Glucocorticoid Receptor, **B.** *Mapt* for Tau, **C.** *GRK2*. **DD.** *HSF1*, **E.** *Fkbp5*, **F.** *CHIP/STUB1*, **G.** *Pin1*, **H.** *CypA*. (N=5/genotype). Data analyzed using Student's t-test.

Supplementary Figure 5. CRISPR/Cas9 STI1 KO SN56 cells have similar disruption of client and cochaperone expression as ΔTPR1 mice. A. Representative Immunoblots for panHsp90, STI1 and Hsp70 expression in SN56 cells. **B-D.** Densitometric quantification of Hsp90, Hsp70 and Hsp90 protein expression relative to WT cells. **E.** Representative **i**mmunoblots for glucocorticoid receptor, STI1 and CHIP in SN56 STI1 KO cells. **F.** Quantification of Glucocorticoid receptor levels **G.** Quantification of CHIP levels. **H.**

Representative Immunoblots for GRK2, FKBP51 and CypA protein levels. **I-K.** Densitometric quantification of protein levels (N=4 dishes). Data analyzed using Student's t-test. All data are Mean ± S.E.M. *p<0.05, **p<0.01, *** p<0.0001.

Supplementary Figure 6. Germ layer markers expressed in differentiated ΔTPR1 mESCs. Representative figure of pluripotency status of embryonic stem cells populations. Detection of three germ layers markers [Ectoderm (BIII-tubulin), mesoderm (anti-sma) and endoderm (anit-alpha-fetoprotein)] in embryoid bodies cells derived from ΔTPR1 blastocytes. **A**. (WT ESCs). **B.** (ΔTPR1 ESCs). Bars: 20µm.

Supplementary Figure 7. Reduced viability and proliferative capacity of ΔTPR1 MEFs. A. Live-Dead Assay in P4 MEFs. Scale bars 100 µm. **B.** Percentage of cell death and **C.** Number of live cells compared to total cells. **D.** Cleaved Caspase-3 (CC-3) in MEFs treated with 150 µM H_2O_2 for 3h. Scale bars 100 µm. **E.** Percentage of CC-3 positive nuclei compared to total nuclei (stained with Hoechst). **F.** MEFs were treated with 30 µM BrdU for 1.5h, (Scale bars 50 µm) and immunofluorescent staining for BrdU was quantified to assess MEF proliferation **G.** (N=4-5 independent MEF cultures/genotype, Data analyzed with Student's t-test). All data are Mean ± S.E.M. *p<0.05, **p<0.01, *** p<0.0001.

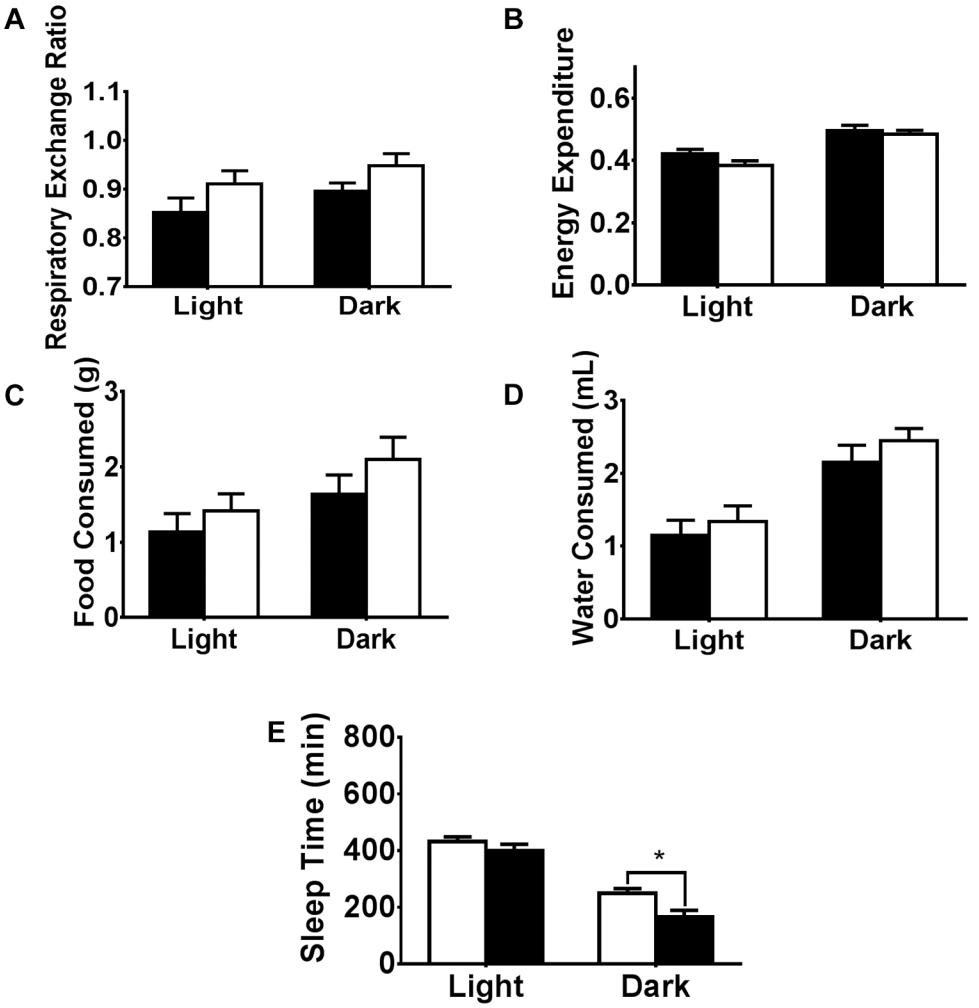

Supplementary Fig. 1

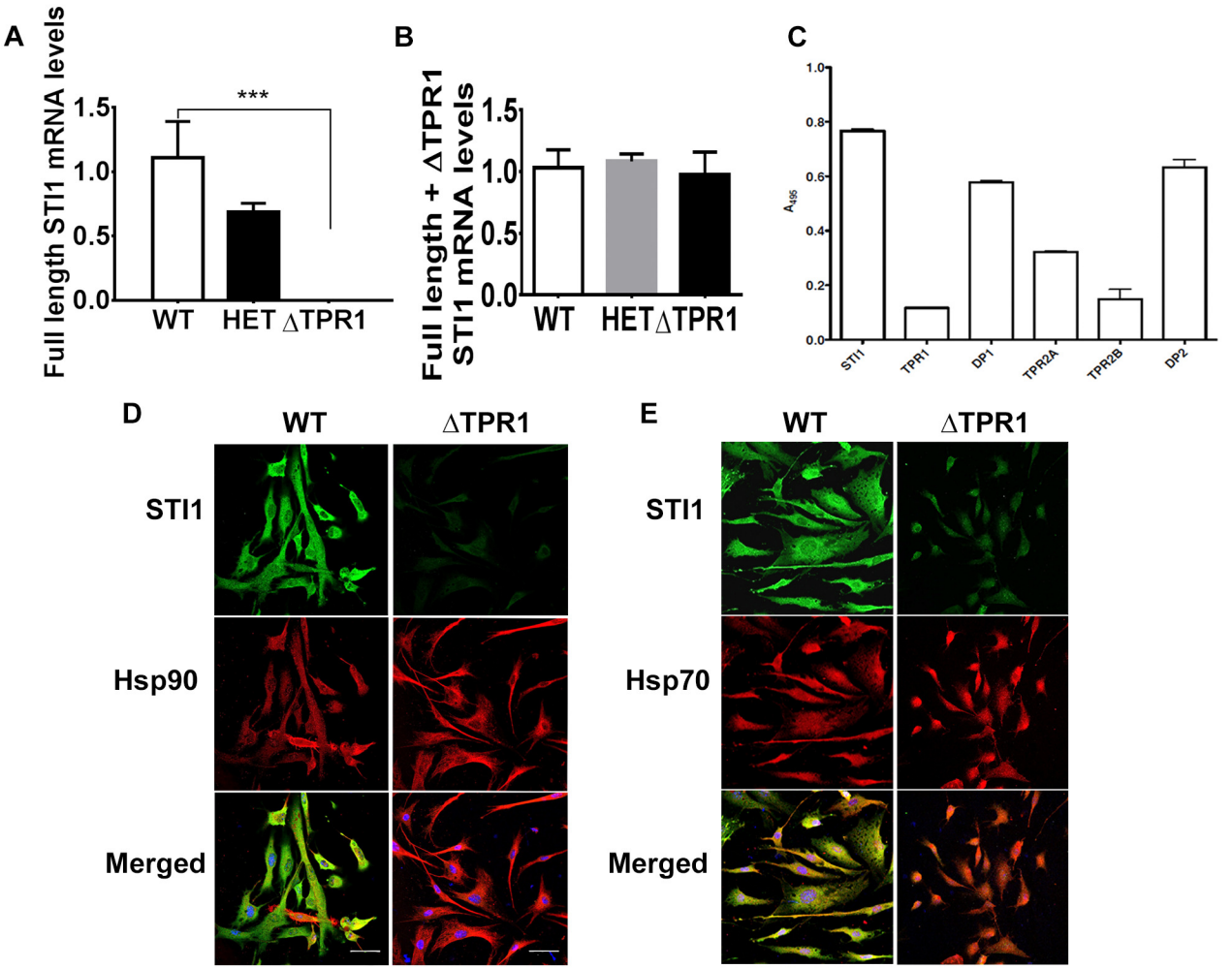

Supplementary Fig. 2

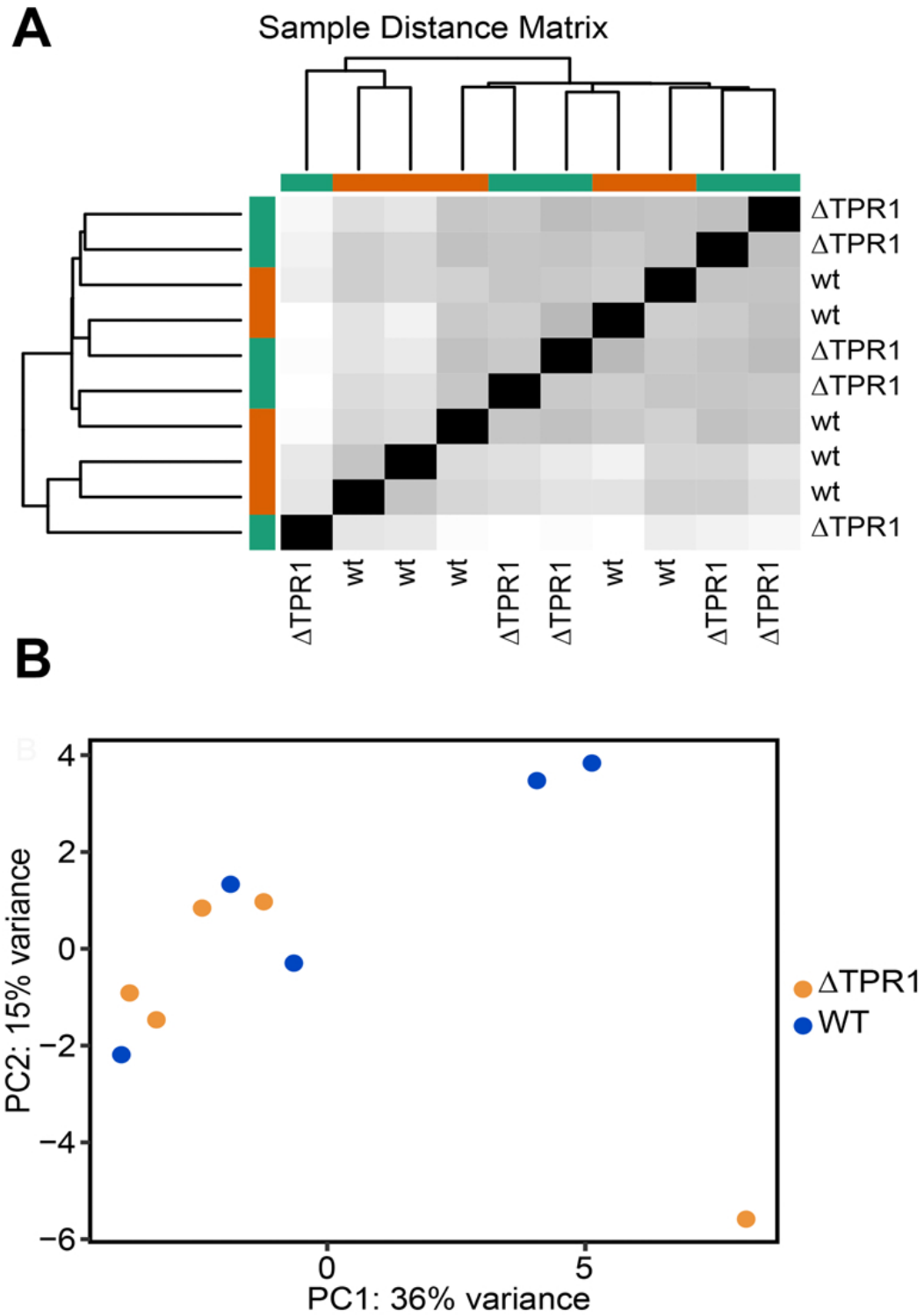

Supplementary Fig. 3

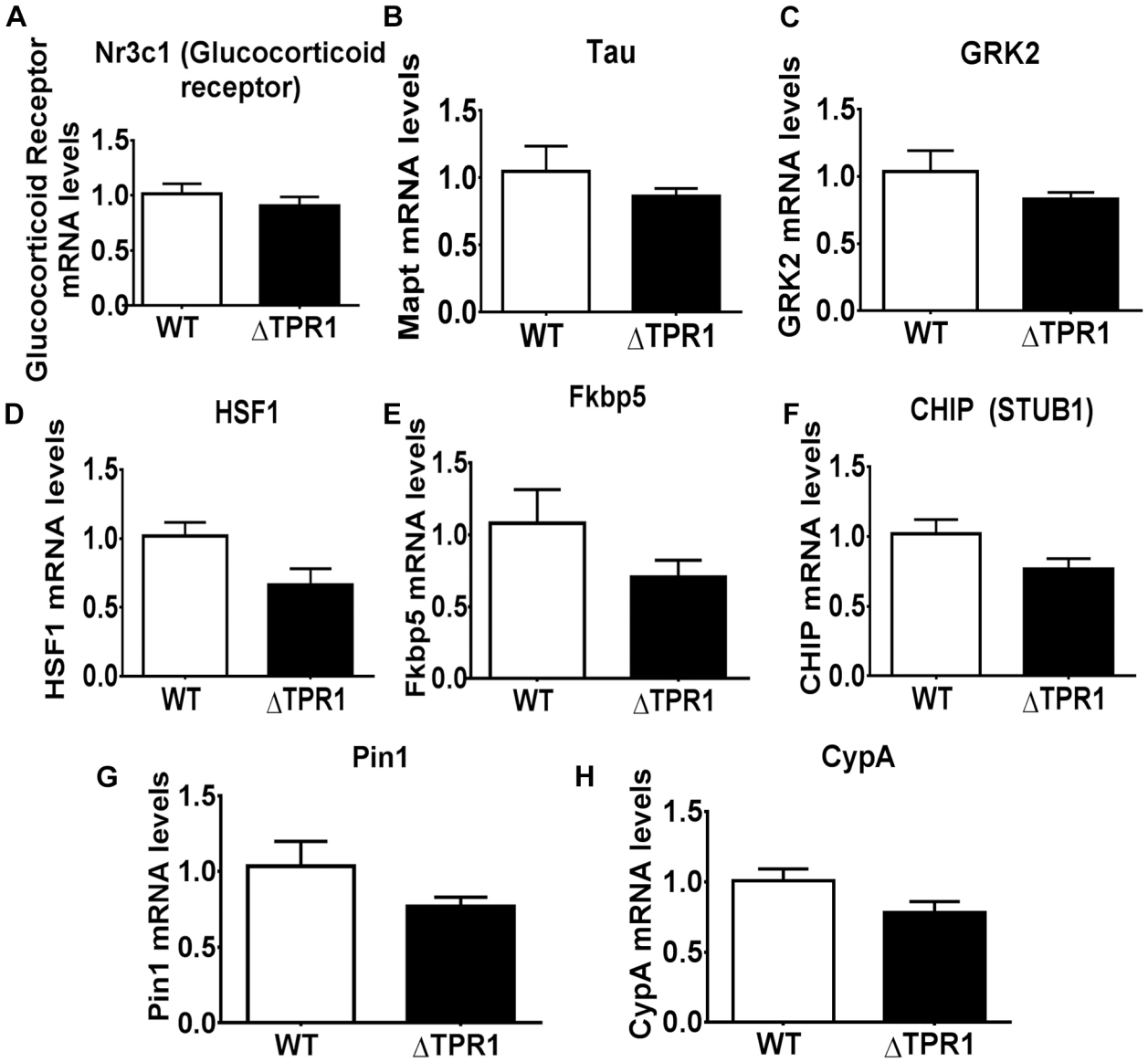

Supplementary Fig. 4

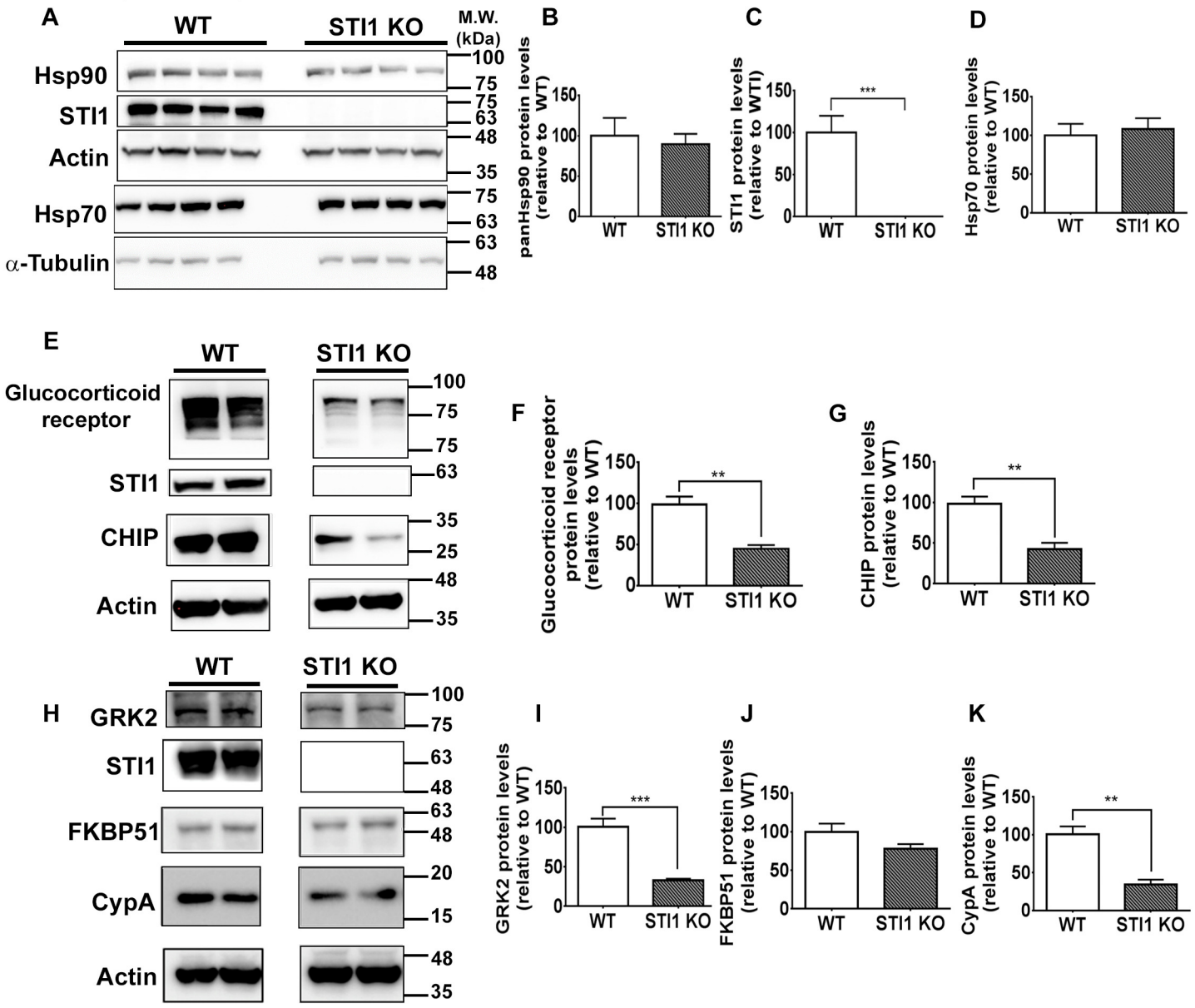

Supplementary Fig. 5

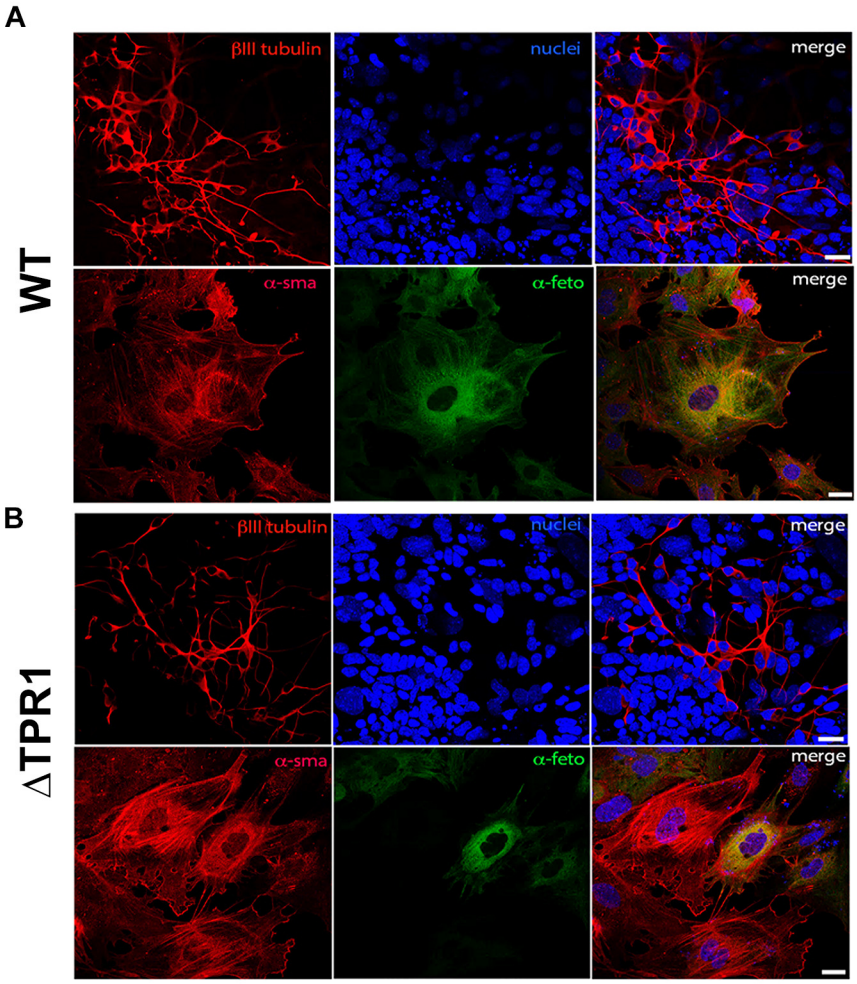

Supplementary Fig. 6

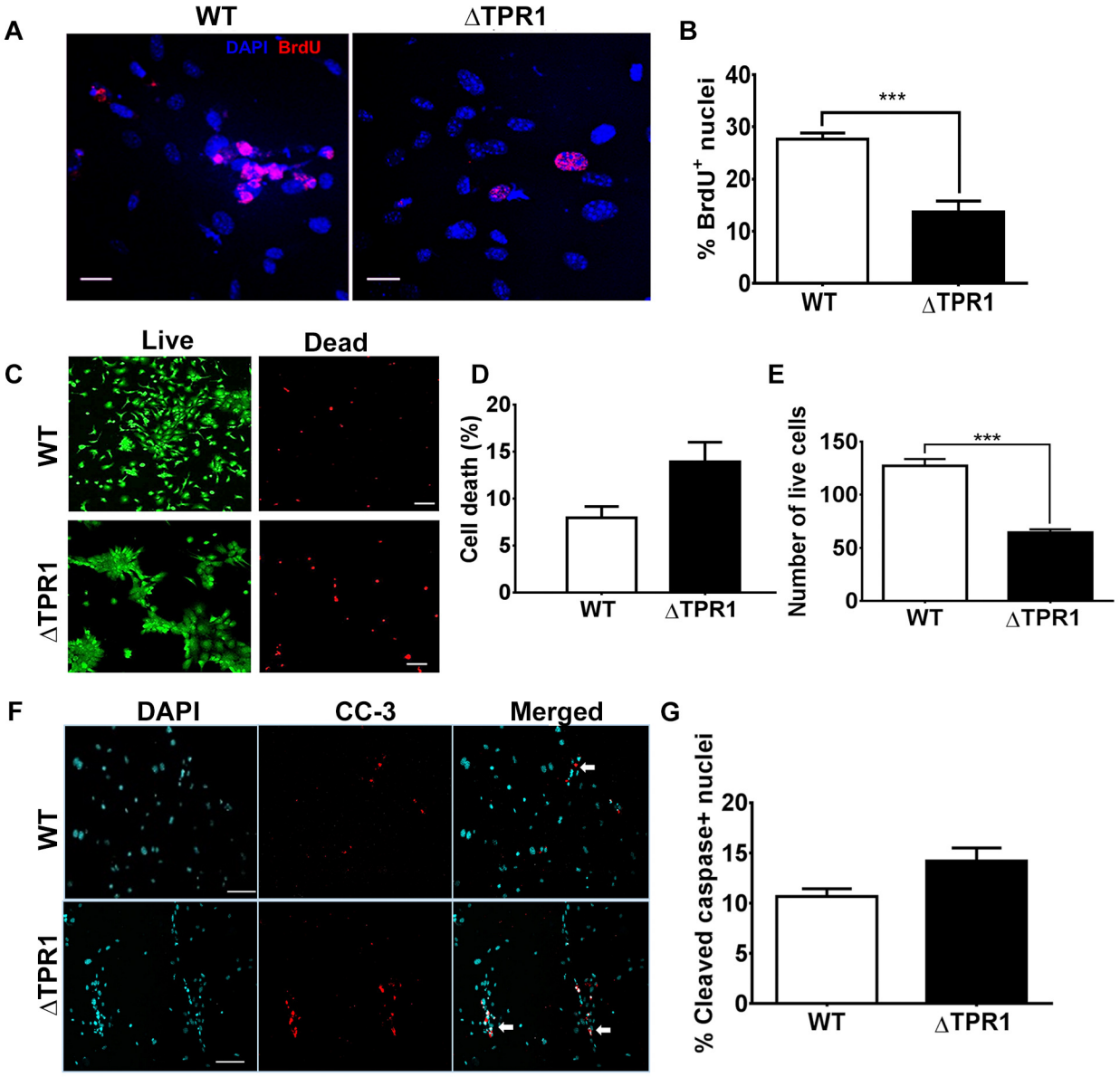

Supplementary Fig. 7

Supplementary Table 1. Genetic information of *STIP1*, *HSP90AA1*, *HSP90AB1*, *PTGES3*, *AHSA1*, *FKBP5*, *PIN1*, *STUB1*, *CDC37*, *PPIA*, *PPP5C*, and *SGTA*, aggregated using publically available databases and repositories of healthy controls and disease-ascertained individuals.

Database	Reference	Type of database (sample size)	Genetic information
ExAC	Lek et al., 2016	Controls (n=60,706)	*STIP1*

- pLI = 1.00, extremely intolerant of loss of function variants
- 10 heterozygous PTVs, 0 homozygous PTVs
- 1 variant likely to be a true PTV

Variant	Frequency
p.Tyr269Ter	1 in 60,650 individuals, 0.000008245%

HSP90AA1

- pLI = 0.68, may tolerate loss of function variants
- 16 heterozygous PTVs, 0 homozygous PTVs
- 8 variants likely to be true PTVs

Variant	Frequency
p.Trp82Ter	1 in 60,702 individuals, 0.00001647%
p.Gln101ArgfsTer22	1 in 60,702 individuals, 0.00001647%
p.Gln107Ter	7 in 60,699 individuals, 0.00005766%
p.Ser287Ter	1 in 60,525 individuals, 0.000008261%
p.Lys372ArgfsTer7	1 in 55,933 individuals, 0.000008939%
p.Arg477LysfsTer18	1 in 60,666 individuals, 0.000008242%
p.Lys479ArgfsTer20	1 in 60,674 individuals, 0.000008241%
p.Lys681SerfsTer16	1 in 60,241 individuals, 0.000008300%

HSP90AB1

- pLI = 1.00, extremely intolerant of loss of function variants
- 4 heterozygous PTVs, 0 homozygous PTVs
- 2 variants likely to be true PTVs

Variant	Frequency
p.Lys481GlufsTer9	1 in 60,695 individuals, 0.000008238%
p.Ser497Ter	1 in 60,706 individuals, 0.000008236%

PTGES3

- pLI = 0.87, may tolerate loss of function variants
- 2 heterozygous PTVs, 0 homozygous PTVs
- 1 variant likely to be a true PTV

Variant	Frequency
p.Glu92GlyfsTer34	1 in 60,233 individuals, 0.000008301%

AHSA1

- pLI = 0.94, extremely intolerant of loss of function variants
- 7 heterozygous PTVs, 1 homozygous PTV
- 0 variants likely to be true PTVs

FKBP5

- pLI = 0.50, may tolerate loss of function variants
- 8 heterozygous PTVs, 0 homozygous PTVs
- 4 variants likely to be true PTVs

Variant	Frequency
p.Asn365LysfsTer16	1 in 60,537 individuals, 0.000008259%
p.Val295AspfsTer20	1 in 60,668 individuals, 0.000008242%
p.Arg39Ter	1 in 60,378 individuals, 0.000008281%
p.Arg31GlyfsTer13	2 in 60,667 individuals, 0.00001648%

PIN1

- pLI = 0.34, may tolerate loss of function variants
- 4 heterozygous PTVs, 0 homozygous PTVs
- 0 variants likely to be true PTVs

STUB1

- pLI = 0.04, may tolerate loss of function variants
- 12 heterozygous PTVs, 1 homozygous PTV
- 5 variants likely to be true PTVs

Variant	Frequency
p.Gln78Ter	1 in 42,473 individuals, 0.00001177%
p.Trp147Ter	1 in 58,268 individuals, 0.000008581%
p.Arg182Ter	1 in 57,185 individuals, 0.000008744%
p.Ile200MetfsTer40	1 in 59,604 individuals, 0.000008389%
p.Tyr230CysfsTer9	1 in 60,065 individuals, 0.000008324%

			CDC37 • pLI = 0.96, extremely intolerant of loss of function variants • 4 heterozygous PTVs, 0 homozygous PTVs • 0 variants likely to be true PTVs
			PPIA • pLI = 0.81, may tolerate loss of function variants • 2 heterozygous PTVs, 0 homozygous PTVs • 0 variants likely to be true PTVs
			PPP5C • pLI = 1.00, extremely intolerant of loss of function variants • 2 heterozygous PTVs, 0 homozygous PTVs • 0 variants likely to be true PTVs
			SGTA • pLI = 0.47, may tolerate loss of function variants • 3 heterozygous PTVs, 0 homozygous PTVs • 0 variants likely to be true PTVs
gnomAD	Lek et al., 2016	Controls (n=138,632)	*STIP1* • 25 heterozygous PTVs, 0 homozygous PTVs • 4 variants likely to be true PTVs

Variant	Frequency
p.Gln25Ter	1 in 123,136 individuals, 4.061e-6%
p.Glu138GlyfsTer3	1 in 123,133 individuals, 4.061e-6%
p.Glu230AlafsTer12	1 in 15,484 individuals, 3.229e-5%
p.Tyr269Ter	1 in 123, 117 individuals, 4.061e-6%

HSP90AA1

• 43 heterozygous PTVs, 0 homozygous PTVs
• 22 variants likely to be true PTVs

Variant	Frequency
p.Pro803SerfsTer6	1 in 15,485 individuals, 3.229e-5%
p.Ala772ArgfsTer9	1 in 122,978 individuals, 4.066e-6%
p.Lys681SerfsTer16	1 in 122,842 individuals, 4.07e-6%

p.Ala625SerfsTer2	1 in 122,960 individuals, 4.066e-6%
p.Glu502Ter	1 in 122,976 individuals, 4.066e-6%
p.Cys496Ter	1 in 15,493 individuals, 3.227e-5%
p.Lys479ArgfsTer20	1 in 123,113 individuals, 4.061e-6%
p.Arg477LysfsTer18	2 in 123,115 individuals, 8.122e-6%
p.Glu351Ter	1 in 121,447 individuals, 4.117e-6%
p.Ile250TyrfsTer19	1 in 122,978 individuals, 4.066e-6%
p.Glu242Ter	1 in 122,971 individuals, 4.066e-6%
p.Phe166Ter	1 in 123,126 individuals, 4.061e-6%
p.Gln145SerfsTer40	1 in 123,126 individuals, 4.061e-6%
p.Glu137AspfsTer17	1 in 123,133 individuals, 4.061e-6%
p.Gln128ProfsTer13	1 in 123,121 individuals, 4.061e-6%
p.Gln128Ter	1 in 15,486 individuals, 3.229e-5%
p.Gln107Ter	11 in 123,128 individuals, 4.467e-5%
p.Gln107AsnfsTer16	1 in 15,486 individuals, 3.229e-5%
p.Gln101ArgfsTer22	7 in 138,619 individuals, 2.525e-5%
p.Trp82Ter	1 in 123,122 individuals, 4.061e-6%
p.Gly39LeufsTer9	1 in 121,701 individuals, 4.108e-6%
p.Asp19ValfsTer25	1 in 15,426 individuals, 3.241e-5%

HSP90AB1

- 14 heterozygous PTVs, 0 homozygous PTVs
- 4 variants likely to be true PTVs

Variant	Frequency
p.Asn100IlefsTer25	1 in 123,132 individuals, 4.061e-6%
p.Tyr457ArgfsTer2	1 in 123,115 individuals, 4.061e-6%
p.Lys481GlufsTer9	1 in 123,117 individuals, 4.061e-6%
p.Ser497Ter	1 in 123,135 individuals, 4.061e-6%

PTGES3

- 4 heterozygous PTVs, 0 homozygous PTVs
- 2 variants likely to be true PTVs

Variant	Frequency
p.Glu92GlyfsTer34	1 in 105,367 individuals, 4.745e-6%
p.Trp86Ter	1 in 15,490 individuals, 3.228e-5%

AHSA1

- 11 heterozygous PTVs, 1 homozygous PTV
- 0 variants likely to be true PTVs

FKBP5

- 14 heterozygous PTVs, 0 homozygous PTVs
- 4 variants likely to be true PTVs

Variant	Frequency
p.Val377CysfsTer4	1 in 123,103 individuals, 4.062e-6%
p.Asn365LysfsTer16	1 in 123,062 individuals, 4.063e-6%
p.Val295AspfsTer20	1 in 123,004 individuals, 4.065e-6%
p.Arg39Ter	1 in 118,791 individuals, 4.209e-6%
p.Arg31GlyfsTer13	2 in 123,012 individuals, 8.129e-6%

PIN1

- 11 heterozygous PTVs, 0 homozygous PTVs
- 1 variants likely to be a true PTV

Variant	Frequency
p.Asn30LysfsTer75	1 in 116,440 individuals, 4.294e-6%

STUB1

- 17 heterozygous PTVs, 1 homozygous PTV
- 4 variants likely to be true PTVs

Variant	Frequency
p.Trp147Ter	1 in 122,320 individuals, 4.088e-6%
p.Ile200MetfsTer40	1 in 122,657 individuals, 4.076e-6%
p.Arg225Ter	2 in 137,975 individuals, 7.248e-6%
p.Tyr230CysfsTer9	2 in 122,785 individuals, 8.144e-6%

CDC37

- 15 heterozygous PTVs, 0 homozygous PTVs
- 2 variants likely to be true PTVs

Variant	Frequency
p.Leu292ProfsTer12	1in 121,779 individuals, 4.106e-6%
p.Ile10LeufsTer59	1 in 122,782 individuals, 4.072e-6%

			PPIA • 16 heterozygous PTVs, 0 homozygous PTVs • 1 variant likely to be a true PTVs **Variant** — **Frequency** c.101-1_101delGA — 2 in 121,215 individuals, 8.25e-6% *PPP5C* • 7 heterozygous PTVs, 0 homozygous PTVs • 1 variant likely to be a true PTVs **Variant** — **Frequency** p.Gln53Ter — 1 in 15,485 individuals, 3.229e-5% *SGTA* • 8 heterozygous PTVs, 0 homozygous PTVs • 0 variants likely to be true PTVs
GWAS Catalog	MacArthur et al., 2017	Cases and controls	*STIP1*
	Mick et al., 2011	Cases and controls (n=341 cases from 339 trios)	• Intron variant, rs11607165-G trending towards association with ADHD (*P*-value $4x10^{-6}$) • Association not replicated
	McGue et al., 2013	Cases and controls (n=7,188)	*HSP90AA1*
			• Intron variant, rs1190596-A trending towards association with nicotine use (*P*-value $4x10^{-6}$) • Association not replicated
	Astle et al., 2016	Cases and controls (n=172,433)	*HSP90AB1*
			• Downstream variant, rs62401155-A may be associated with mean corpuscular volume (*P*-value 6 $x10^{-11}$) • Association not replicated
	Gieger et al., 2011	Cases and controls (n=66,867 individuals from 36 studies)	*PTGES3*
			• Downstream variant, rs2950390-C may be associated with mean platelet volume (*P*-value $7.45x10^{-14}$)

		• Downstream variant, rs941207-G may be associated with platelet count (*P*-value $2x10^{-}10$) • Associations not replicated
		AHSA1
		• No association reported
Astle et al., 2016	Cases and controls (n=172,435)	*FKBP5*
		• Intron variant, rs7760951-C may be associated with eosinophil percentage of white cells (*P*-value $1x10^{-}11$) • Intron variant, rs7760951-C may be associated with white blood cell count (*P*-value $1x10^{-}11$) • Intron variant, rs7760951-C may be associated with eosinophil percentage of granulocytes (*P*-value $1x10^{-}10$) • Associations not replicated
Gottlieb et al., 2014	Cases and controls (n=47,180)	*PIN1*
		• 3'UTR variant, rs2287838 may be associated with sleep duration (*P*-value $1x10^{-}7$) • Association not replicated
		STUB1
		• No association reported
		CDC37
		• No association reported
		PPIA
		• No association reported
Astle et al., 2016	Cases and controls (n=172,435)	*PPP5C*
		• Synonymous variant, rs61747094-A may be associated with basophil percentage of white cells (*P*-value $2x10^{-}9$) • Association not replicated
		SGTA

			• No association reported
ClinVar	Landrum et al., 2016	Cases (n=519,321 submissions)	*STIP1*
	Miller et al., 2010	Cases (n=21,698 patients from 33 studies)	• Copy number gain in 11p15.5-q25; and loss in 11q12.3-13.1 (>1000 genes implicated in some cases) in patients with abnormal morphology and developmental disabilities. • Copy number gain and loss are classified as 'pathogenic' or 'likely pathogenic'. • No variants in only *STI1*.
			HSP90AA1
	Miller et al., 2010	Cases (n=21,698 patients from 33 studies)	• Copy number gain in 14q11.2-32.33, 14q24.2-32.33, 14q23.2-32.33, 14q32.2-32.33, 14q32.12-32.33, 14q24.3-32.33, 14q31.3-32.33, 14q31.2-32.33; and loss in 14q32.2-32.33, 14q32.31-32.33, 14q32.2-32.31, 14q32.13-32.33 (>1000 genes implicated in some cases) in patients with abnormal developmental delay and/or other significant developmental or morphological phenotypes. • Copy number gain and loss are classified as 'pathogenic'. • No variants in only *HSP90AA1*.
			HSP90AB1
	Miller et al., 2010	Cases (n=21,698 patients from 33 studies)	• Copy number gain in 6p25.3-q27, 6p25.3-12.3; and loss in 6p21.1-12.3, 6p21.2-12.3 (>100 genes implicated in some cases) in patients with short stature, abnormality of cardiovascular system morphology, abnormality of the ear, polydactyly, developmental delay and/or other significant developmental or morphological phenotypes. • Copy number gain and loss are classified as 'pathogenic'. • No variants in only *HSP90AB1*.
			PTGES3
	Miller et al., 2010	Cases (n=21,698 patients from 33 studies)	• Copy number gain in 12p13.33-q24.33 (>1000 genes implicated in some cases) in patients with short stature, abnormality of cardiovascular system morphology, abnormality of the ear, and/or polydactyly.

			• Copy number gain is classified as ‘pathogenic’. • No variants in only *PTGES3*.
			AHSA1
	Miller et al., 2010	Cases (n=21,698 patients from 33 studies)	• Copy number gain in 14q11.2-32.33, 14q24.2-32.33, 14q23.2-32.33, 14q24.3-32.33; and loss in 14q24.2-24.3, 14q24.3-31.1, 14q24.1-31.1, 14q24.3 (>1000 genes implicated in some cases) in patients with short stature, abnormality of cardiovascular system morphology, abnormality of the ear, polydactyly, laryngotracheomalacia, muscular hypotonia, and/or other significant developmental or morphological phenotypes. • Copy number gain and loss are classified as ‘pathogenic’ or ‘likely pathogenic’. • No variants in only *AHSA1*.
			FKBP5
	Miller et al., 2010	Cases (n=21,698 patients from 33 studies)	• Copy number gain in 6p25.3-q27, 6p25.3-12.3 (>1000 genes implicated in some cases) in patients with short stature, abnormality of cardiovascular system morphology, abnormality of the ear, polydactyly, and/or other significant developmental or morphological phenotypes. • Copy number gain are classified as ‘pathogenic’. • No variants in only *FKBP5*.
			PIN1
	Miller et al., 2010	Cases (n=21,698 patients from 33 studies)	• Copy number gain in 19p13.3-q13.43, 19p13.2-13.12, 19p13.2; and loss in 19p13.2 (>1000 genes implicated in some cases) in patients with short stature, abnormality of cardiovascular system morphology, abnormality of the ear, polydactyly, and/or global developmental delay. • Copy number gain are classified as ‘pathogenic’ or ‘likely pathogenic’. • No variants in only *PIN1*.
			STUB1
	Miller et al., 2010	Cases (n=21,698 patients from 33 studies)	• Copy number gain in 16p13.3-13.2, 16p13.3, 16p13.3-12.2, 16p13.3-q24.3, 16p13.3-12.3, 16p13.3-13.2, 16p13.3-11.2, 16p13.3-13.11, 16p13.3-13.12,

		16p13.3-13.13; and loss in 16p13.3 (>200 genes implicated in some cases) in patients with significant developmental or morphological phenotypes. • Copy number gain and loss are classified as 'pathogenic' or 'likely pathogenic'.
Heimdal et al., 2014 Synofzik et al., 2014 Shi et al., 2013 Shi et al., 2014	2 families, 4 patients 300 patients 3 families, 6 patients 1 family, 2 patients	• 12 variants in *STUB1*, classified as 'pathogenic' or 'likely pathogenic' associated with autosomal recessive spinocerebellar ataxia: p.Asn65Ser, p.Ala79Thr, p.Ala79Asp, p.Leu123Val, p.Asn130Ile, p.Trp147Cys, p.Leu165Phe, p.Ser216Phefs, p.Cys232_Gly233del, p.Met240Thr, p.Arg241Gly, and p.Thr246Met.
		CDC37
Miller et al., 2010	Cases (n=21,698 patients from 33 studies)	• Copy number gain in 19p13.3-q13.43, 19p13.2-13.12, 19p13.2-13.13; and loss in 19p13.2 (>30 genes implicated in some cases) in patients with short stature, abnormality of cardiovascular system morphology, abnormality of the ear, polydactyly, and/or global developmental delay. • Copy number gain are classified as 'pathogenic' or 'likely pathogenic'. • No variants in only *CDC37*.
		PPIA
Miller et al., 2010	Cases (n=21,698 patients from 33 studies)	• Copy number gain in 7p22.3-q36.3, 7p21.3-12.1, 7p14-q11.21 and loss in 7p22.3-q36.3, 7p14.1-12.3, 7p14.1-13, 7p14.1-12.1, 7p14.1-11.2, 7p13-12.1, 7p13-12.3 (>200 genes implicated in some cases) in patients with micrognathia, ventricular septal defect, abnormal facial shape, syndactyly, intrauterine growth retardation, intellectual disability, macrocephaly, and/or global developmental delay. • Copy number gain are classified as 'pathogenic'. • No variants in only *PPIA*.
		PPP5C
Miller et al., 2010	Cases (n=21,698 patients from 33 studies)	• Copy number gain in 19p13.3-q13.43, 19q13.32; and loss in 19q13.32-13.33, 19q13.2-13.32, 19q13.32 (>40 genes implicated in some cases) in patients with short stature, abnormality of cardiovascular system morphology, abnormality of the ear, polydactyly, dyslexia, anxiety, and/or tremor.

			• Copy number gain are classified as ‘pathogenic’ or ‘likely pathogenic’. • No variants in only *PPP5C*.
			SGTA
	Miller et al., 2010	Cases (n=21,698 patients from 33 studies)	• Copy number gain in 19p13.3-q13.43, 19p13.3, 19p13.3-13.2; and loss in 19p13.3 (>90 genes implicated in some cases) in patients with short stature, abnormality of cardiovascular system morphology, abnormality of the ear, polydactyly, developmental delay and/or other significant developmental or morphological phenotypes. • Copy number gain are classified as ‘pathogenic’ or ‘likely pathogenic’. • No variants in only *SGTA*.
DECIPHER	Firth et al., 2009	Cases (n=24,999 patient records)	*STIP1*
		Cases (n= 6)	• Copy number gain in 11q12.2-13.1, 11p11.2-q25; and loss in 11q12.3-13.1, 11p15.5-q25 (>1500 genes implicated in some cases) in patients with abnormal morphological phenotypes and/or developmental delay. • Copy number gain and loss are classified as ‘pathogenic’ or ‘likely pathogenic’. • No variants in only *STI1*.
			HSP90AA1
		Cases (n=17)	• Copy number gain in 14q32.11-32.33, 14q32.31-32.32, 14q32.13-32.33, 14q32.12-32.33; and loss in 14q32.1-32.33, 14q32.2-32.33, 14q32.31-32.33 (>400 genes implicated in some cases) in patients with abnormal morphological phenotypes and/or global developmental delay. • Copy number gain and loss are classified as ‘pathogenic’ or ‘likely pathogenic’. • No variants in only *HSP90AA1*.
			HSP90AB1

	Cases (n=4)	• Copy number gain in 6p25.3-q13; and loss in 6p21.2-21.1, 6p21.1-12.3 (>30 genes implicated in some cases) in patients with abnormal morphological phenotypes and/or global developmental delay. • Copy number gain and loss are classified as 'likely pathogenic'. • No variants in only *HSP90AB1*.
		PTGES3
	Cases (n=4)	• Copy number gain in 12q13.13-14.3, and loss in 12p13.31-q24.33 (>180 genes implicated in some cases) in patients with abnormal facial shape and global developmental delay. • Copy number gain and loss are classified as 'pathogenic' or 'likely pathogenic'. • No variants in only *PTGES3*.
		AHSA1
		• No association with classifications as 'pathogenic' or 'likely pathogenic' reported.
		FKBP5
	Cases (n=2)	• Copy number gain in 6p25.3-q13 (>900 genes implicated in some cases). Patient phenotype not reported. • Copy number gain is classified as 'likely pathogenic'. • No variants in only *FKBP5*.
		PIN1
	Cases (n=1)	• Copy number loss in 19p13.2 (>100 genes implicated) in patients with abnormality of the nasolacrimal system, ankyloglossia, atria septal defect, behavioral abnormality, brachydactyly syndrome, hypospadias, intellectual disability, low hanging columella, microdontia, prominent nasal bridge, sacral dimple, single transverse palmar crease, and sleep disturbance. • Copy number loss is classified as 'pathogenic'. • No variants in only *PIN1*.

		STUB1
	Cases (n=14)	• Copy number gain in 16p13.3-13.2, 16p13.3-13.11, 16p13.3, and loss in 16p13.3 (>50 genes implicated in some cases) in patients with morphological abnormalities, learning disability, obesity, autism, and/or global developmental delay. • Copy number gain and loss are classified as 'pathogenic' or 'likely pathogenic'. • No variants in only *STUB1*.
		CDC37
	Cases (n=1)	• Copy number loss in 19p13.2 (>100 genes implicated in some cases) in patients with abnormality of the nasolacrimal system, ankyloglossia, atria septal defect, behavioral abnormality, brachydactyly syndrome, hypospadias, intellectual disability, low hanging columella, microdontia, prominent nasal bridge, sacral dimple, single transverse palmar crease, and sleep disturbance. • Copy number loss is classified as 'pathogenic'. • No variants in only *CDC37*.
		PPIA
	Cases (n=4)	• Copy number gain in 7p14.1-q11.22, loss in 7p15.3-11.2, 7p14.3-12.3, 7p14.1-11.2 (>90 genes implicated in some cases) in patients with morphological abnormalities and/or intellectual disability. Phenotypes not reported for 2 patients. • Copy number gain and loss are classified as 'pathogenic' or 'likely pathogenic'. • No variants in only *PPIA*.
		PPP5C
	Cases (n=1)	• Copy number loss in 19q13.31-13.32 (>60 genes implicated) in patients with bipolar affective disorder, broad-based gait, cataract, intellectual disability, mild, seizures, and short nose.

		• Copy number loss is classified as ‘pathogenic’. • No variants in only *PPP5C*.
		SGTA
	Cases (n=8)	• Copy number gain in 19p13.3-13.2, 19p13.3, and loss in 19p13.3 (>40 genes implicated in some cases) in patients with morphological abnormalities and/or global developmental delay. • Copy number gain and loss are classified as ‘pathogenic’ or ‘likely pathogenic’. • No variants in only *SGTA*.

Abbreviations are as follows: ExAC, Exome Aggregation Consortium; gnomAD, Genome Aggregation Database; GWAS, genome-wide association study; DECIPHER, DatabasE of genomiC varIation and Phenotype in Humans using Ensembl Resources; PTV, protein truncating variant; these types of genetic variants typically cause the gene to lose its intended function unless they are within the last exon of the gene, and are likely to escape non-sense mediated decay. pLI, probability of loss of function intolerance score. A pLI score >0.9 indicates loss of function in a given gene is not tolerated. Controls are referred to individuals who are part of public databases that are controls for the majority of studies; cases are referred to individuals who were ascertained for a specific disease. Importantly, not all controls are healthy; however, they do not have a Mendelian disease.

Supplementary Table 2

Stage	***WT***	***WT/ΔTPR1 (HET)***	***ΔTPR1***	***Total***
Live Birth	28.9%	56.1%	15%	246***

Supplementary Table 3

Stage	***WT***	***KO/WT***	***KO/ΔTPR1***	***WT/ΔTPR1***	***Total***
Live Birth	9	11	2	32	54